https://doi.org/10.5194/egusphere-2025-1169
Preprint. Discussion started: 13 June 2025

Landslide Hazard Microzonation Using a Hybrid Integrated Approach to Reduce Disaster Risk: A Case Study of Jecheon, South Korea

Jae-Joon Lee[1], Manik Das Adhikari[2], Moon-Soo Song[2], Sang-Guk Yum[2]*

[1] Department of Fire Safety Engineering, Jeonju University, Jeonju, Jeollabuk-do, Republic of Korea

[2] Department of Civil and Environmental Engineering, Gangneung-Wonju National University, Gangneung, Gangwon-do, Republic of Korea

**Corresponding author: Sang-Guk Yum; skyeom0401@gwnu.ac.kr*

Abstract

Effective landslide prevention and mitigation necessitate the development of reliable landslide susceptibility map. However, previous studies have primarily focused on assessing the overall performance of predicted susceptibility rather than examining the spatial characteristics of the predicted Landslide Susceptibility Index (LSI). This study aims to evaluate the efficacy of predicted LSIs derived from widely used statistical models while considering the spatial characteristics of landslides. To achieve this goal, four commonly used LSI models, namely frequency ratio (FR), certainty factor (CF), logistic regression (LR), and information value (IV), were utilized to map landslide susceptibility in Jecheon, South Korea. The models were developed using 112 landslide inventories and taking into account topography, hydrogeology, soils, forests, and lithological heterogeneities. Subsequently, the predicted LSIs were compared with the 1D topography profiles of recent landslide events delineated from the high-resolution aerial and drone imagery. The distribution of anticipated LSIs along the landslide source area to the landslide runout and deposit zones was found to be inconsistent with the landslide characteristics. Nevertheless, the overall accuracy of the FR, IV, CF, and LR models demonstrated the strong predictive capabilities of these models. To address this spatial inconsistency issue, we proposed a hybrid integrated approach to achieve higher accuracy than the individual LSI models. Subsequently, a landslide hazard microzonation map was prepared and validated based on the in-situ observations and inventory data. It was observed that 94.6% of landslide inventory occurrences fell within severe to high-hazard zones. Precision results, such as an area under the curve of 0.906, mean square error of 0.25, mean absolute error of

https://doi.org/10.5194/egusphere-2025-1169
Preprint. Discussion started: 13 June 2025

0.08, root mean square error of 0.28, and a precision of 88.3%, suggest that the hybrid integrated approach is more useful for landcover planning and mitigating landslide-induced disaster risks compare to individual LSI models.

Keywords: Landslide susceptibility, Logistic regression, Certainty factor, Frequency ratio, Information value, Hybrid Integrated approach, Accuracy

1. Introduction

Landslides are geologic events in which large amounts of soil and rock detach from the ground and move downslope, potentially causing damage and destruction in their path. The damage caused by landslides is critical on a global scale. During the last century, landslides have resulted in thousands of fatalities and billions of dollars in property damage (Chen and Chen, 2020; Lee et al., 2017). Due to high-intensity rainfall and a changing climate, landslides have become more frequent in recent years (Lee et al., 2018). Consequently, numerous researchers (Dash et al., 2022; Mandal et al., 2021; Pham et al., 2020; Shano et al., 2020; Zhou et al., 2018; Aditian et al., 2018; Ghosh and Bhattacharya, 2010) have pursued work to predict and prevent landslide hazards using various methods.

The Korean peninsula's geological fragility, mountainous topography, and frequent typhoon-induced heavy rainfall make it prone to deadly landslides. In recent decades, these landslides have caused significant loss of life and property damage. Lee and Winter (2019) reported that more than 1728 fatalities occurred between 1970 and 2017 in the Korean peninsula and an annual financial loss of about US$ 500M due to landslides. In South Korea, a large population resides in landslide susceptible regions (Lee et al., 2002). In addition, it is anticipated that climate change, urbanization, and timber harvesting will increase the frequency and severity of landslide-induced damages (Park et al., 2019). Therefore, a reliable landslide hazard potential mapping is crucial in understanding the fundamental concepts of risk assessment and its impact.

The landslide hazard microzonation assesses the potential for natural slope instability in a given area (Peethambaran and Leshchinsky, 2023). It involves evaluating the physical factors that can lead to landslides and creating a map to show the relative likelihood of such an event occurring in a given area. The resulting landslide susceptibility maps indicate the regions most likely to experience landslides (Guzzetti et al., 1999). In the past two decades, several statistical and machine-learning models for landslide susceptibility analysis have been

https://doi.org/10.5194/egusphere-2025-1169
Preprint. Discussion started: 13 June 2025

suggested, presuming that landslides trigger in a similar environment to prior landslides (Wei et al., 2023; Reichenbach et al., 2018; Park et al., 2013; Lee and Pradhan, 2007; Lee et al., 2002). Although numerous techniques have been put forth to create GIS-based landslide susceptibility maps, there still needs to be an agreement on the best practices (Aditian et al., 2018). Most quantitative methods considered past landslides to determine the ranks and weight of each factor attribute based on their spatial association. Subsequently, several quantitative methods, including frequency ratios, Shannon entropy, certainty factor, logistic regression, information value, weights of evidence, support vector machine, neural networks, random forest, and hybrid models, are frequently applied to landslide potential mapping (e.g., Park et al., 2023; Dash et al., 2022; Mandal et al., 2021; Pham et al., 2020; Aditian et al., 2018; Riaz et al., 2018; Zêzere et al., 2017; Shahabi and Hashim, 2015; Wang et al., 2015). The benefits and drawbacks of several probabilistic and statistical approaches were recently reviewed by Merghadi et al. (2020) and Shano et al. (2020). Even though there were numerous studies on landslide susceptibility, no single approach is suitable for all cases. As a result, to determine landslide susceptibility in a given area, the best model must be chosen based on the landslide's characteristics and the accessibility of inventory data (Zhu et al., 2018). Consequently, it is still crucial to calculate the effectiveness of various models for particular landslide susceptibility procedures. In addition, model integration provides another opportunity to improve model accuracy by combining different models on the GIS platform.

A landslide susceptibility index typically indicates areas that are more prone to landslides based on various factors and parameters. Thus, previous studies have primarily focused on assessing the overall performance of predicted susceptibility rather than examining the spatial characteristics of the predicted Landslide Susceptibility Index (LSI). The overall accuracy of widely accepted models may produce acceptable LSIs in terms of AUC, MAE, and RMSE, but they may not always be comparable with the landslide characteristics. For example, the landslide source area is the region at the top of a slide where the slope begins to fail, and the movement of the soil, rock, and other material begins (Lee et al., 2002). Thus, the predicted LSI value should be higher in the source and crown zones. On the other hand, the landslide deposit area is the region at the bottom of the slide, where the material from the source area ends up after it has moved downslope and poses further vulnerability. Consequently, the LSI value in the landslide-deposited area must be lower than the source area. Therefore, the landslide characteristics along with the AUC, MAE and RMSE, should be used to validate the predicted LSI values (Lee et al., 2002). However, most landslide studies consider the overall

https://doi.org/10.5194/egusphere-2025-1169
Preprint. Discussion started: 13 June 2025

model performance (i.e., AUC) and ignore the spatial inconsistency phenomenon. Therefore, the main novelties of this study include (a) the development of landslide susceptibility (LSI) maps by comparing and analyzing different statistical models commonly used for assessing LSI, (b) evaluating spatial characteristics of the predicted landslide susceptibility indexes to study previously overlooked accuracy criteria, (c) proposed a hybrid integrated approach to achieve higher accuracy than the individual LSI models, and (d) prepared a reliable landslide hazard microzonation map to mitigate landslide-induced disaster risks appropriately.

2. Study area

The mountainous region of South Korea is prone to rainfall-induced landslides, causing fatalities and extensive damage to roads, bridges, and settlements. Over 70% of the Korean peninsula has steep mountain slopes (>30°) (Lee et al., 2022a; Lee et al., 2015). Rainfall accompanied by occasionally severe typhoons has adversely affected this region (Lee et al., 2022b). In contrast, shallow landslides often occur throughout the rainy season (June to September) under different geological conditions (Kim et al., 2021). According to the Korea Forestry Service's analysis of landslide extent, the annual average landslide area rapidly increased from 231 hectares in the 1980s to 713 hectares in the 2000s (Lee et al., 2018). The present work focuses on the Jecheon-si region (36°48′47"-37°16′ 15"N, 127°55′19"-128°20′ E), situated in the northern part of North Chungcheong Province and covers an area of ~ 884.3372 km^2 (Fig. 1). This region is surrounded by mountains, lake (Cheongpung Lake) and reservoirs. Geologically, the region is situated in the southwestern part of the Gyeonggi Massif, which is composed of the metamorphic basement and sedimentary strata (Seo et al., 2011). The surface geology is mainly covered by sandy mudstone, mudstone, quaternary loess strata outcrop and sandstone (Jung and Kang, 2014; Kihm et al., 2000). The topography of Jecheon-si is mainly composed of mountains with the highest altitude of 1157m and the lowest elevation of 117m. The city exhibits dispersed high-density settlements (Fig. 1b), which makes it very densely populated in some areas. The original terrain was altered during the urbanization due to engineering activities (i.e., road construction), resulting in slope deformation and instability in this region.

https://doi.org/10.5194/egusphere-2025-1169
Preprint. Discussion started: 13 June 2025

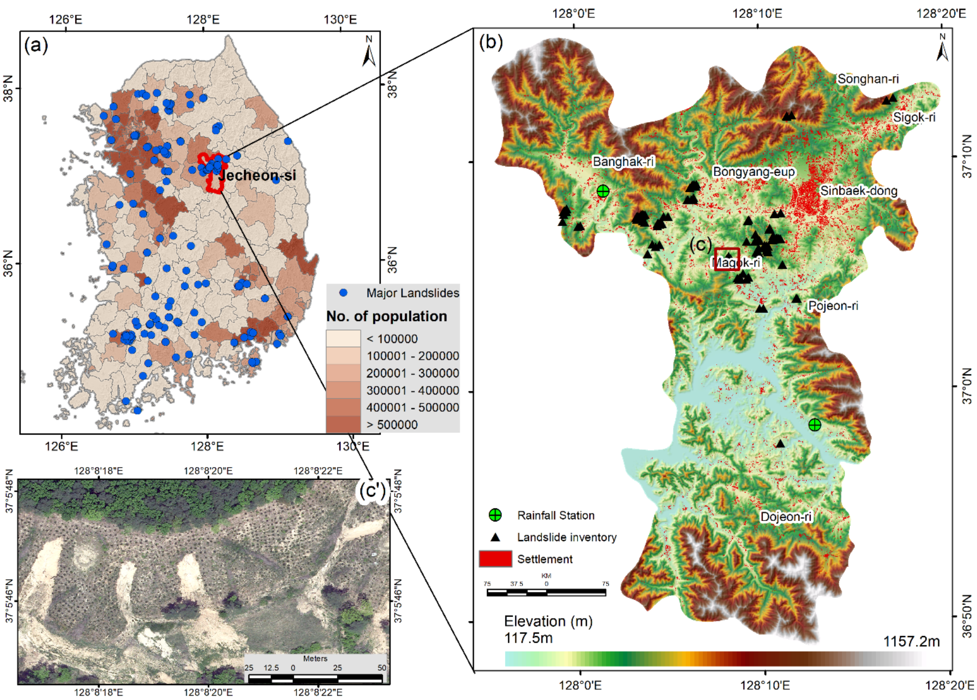

Fig. 1 Location of the study area (Jecheon-si): **a** major landslide distribution of South Korea during 2007-2020 reported by Lee et al. (2022b), **b** updated landslide inventory of Jecheon-si region, and **c** typical landslide detected from the aerial photo (aerial image acquisition 2021, http://map.ngii.go.kr/ms/map/).

Jecheon region receives 1,360.9mm of rainfall annually. The highest rainfall in a single month was 265.2mm in August, and the lowest amount recorded in a single month was 26.9mm in February. Rain can cause various changes in the soil, including increased saturation and decreased stability. Increased saturation can cause the soil to become more prone to slippage and movement, while decreased stability can lead to soil becoming more susceptible to erosion (Pradhan and Kim, 2016). Additionally, heavy rainfall can trigger landslides by loosening rocks and debris on steep slopes (Pradhan and Kim, 2014). Furthermore, intense rainstorms can also cause streams and rivers to swell rapidly, leading to increased erosion and landslide risk. The region is likely to have an increased risk of landslides when there is high-intensity rainfall in a short period, especially during August and September when the most rainfall is recorded, as observed in 2020 (Lee et al., 2022b). In the present study, the short-term rainfall characteristics were analyzed in the past 28 days before the recorded landslide event on 3rd August 2020, at

https://doi.org/10.5194/egusphere-2025-1169
Preprint. Discussion started: 13 June 2025

Jung-myeon, and 2nd August 2020, at Wonbak-ri, in the Jecheon-si region as depicted in Fig. 2. We obtained rainfall data from the automatic weather station (AWS) (https://data.kma.go.kr/) located in Jecheon-si on a daily basis (Fig. 1b). At both sites, the accumulated rainfall was 536mm and 514.5mm, respectively, before the recorded landslide event.

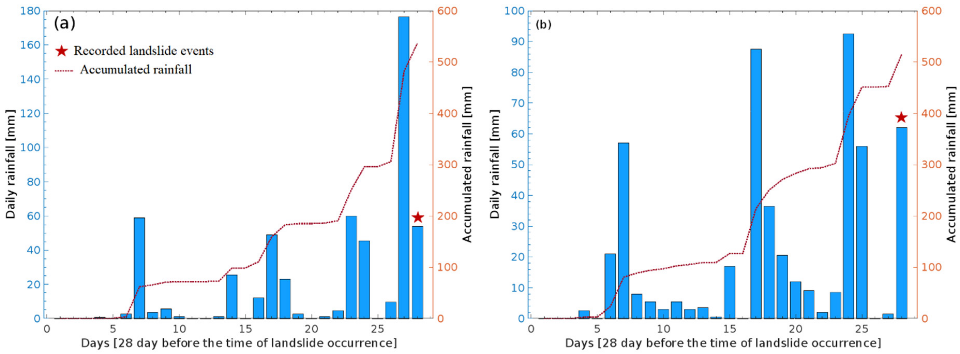

Fig. 2 Rainfall characteristics in the past 28 days before the recorded landslide event on **a** 3rd August 2020, at Jung-myeon, and **b** 2nd August 2020, at Wonbak-ri, in the Jecheon-si region (Data Source: https://data.kma.go.kr/).

3. Data and methods

Landslide susceptibility analysis was performed using the FR, CF, IV, and LR models based on spatial and non-spatial data. This study used the following steps to analyze landslide susceptibility: (1) creating spatial data on landslide predisposing factors and a detailed landslide inventory database, (2) the relationship between landslide predisposing factors and inventory analyzed using the FR model, (3) the FR, IV, CF and LR models were performed using MATLAB and ArcGIS software, (4) comprising of predicted LSI values with the topographic and landslide characteristics of a few past landslide events, and (5) integration of four LSI models (i.e., FR, IV, CF and LR) on the GIS platform and evaluated the accuracy of integrated and individual models using R-Index, RMSE, MAE, MSE and ROC. The workflow of this study is shown in Fig. 3. The detailed data and methods used in the present study were discussed in sections 3.1 and 3.2.

https://doi.org/10.5194/egusphere-2025-1169
Preprint. Discussion started: 13 June 2025

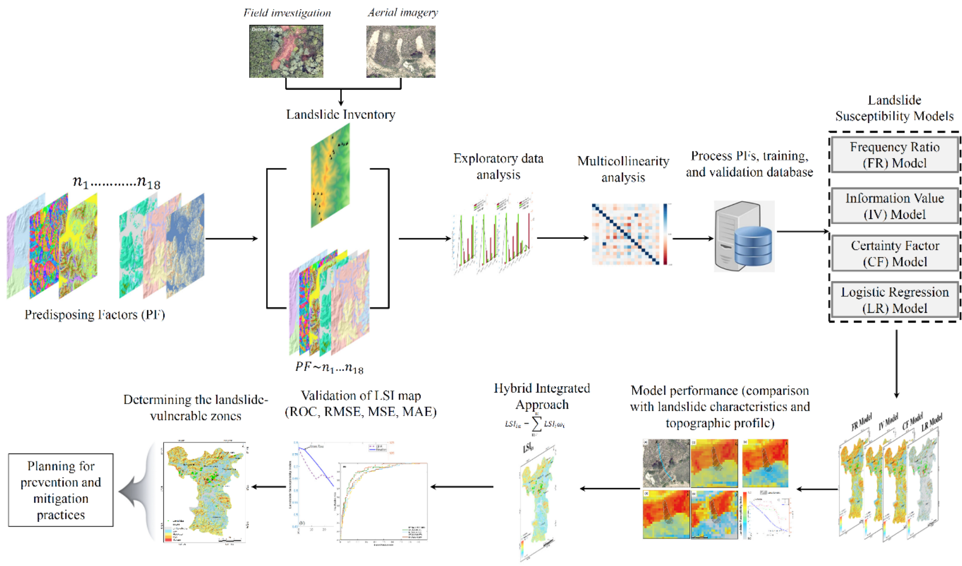

Fig. 3 Workflow of the analytical framework and detailed steps of landslide hazard microzonation mapping proposed in the present study.

3.1. Landslide inventory and predisposing factors

3.1.1 Preparation of landslide inventory database

A landslide inventory database presents the location and characteristics of prior landslides. Thus, the inventory map offers valuable information regarding the spatial and temporal distribution of existing slope failures and the potential of future slides (Choi et al., 2012). Conversely, creating an inventory database is essential for evaluating the accuracy statistics of landslide potential maps (Park et al., 2019). In order to create a landslide inventory database, various methods can be employed, including field assessments, satellite imagery, and aerial photography. In the present study, the inventory database was created using aerial photographs (available at http://map.ngii.go.kr/ms/map/), historical Google Earth imagery, and field investigation. The best way to get an image of a landslide inventory is to use Google Earth (Kadavi et al., 2018; Van Den Eeckhaut et al., 2012). Google Earth is a powerful tool allowing users to view satellite imagery and aerial photographs of a location on a multi-temporal scale. In addition, the boundaries of the landslides were mapped using dronographs and aerial imageries. The landslide boundary is presented using polygon data, and point data indicate the landslide crown zones, source areas, runout and depositional areas, as depicted in Fig. 4. Subsequently, we detected 112 landslides spread over the Jecheon-si region, as shown in Fig.

https://doi.org/10.5194/egusphere-2025-1169
Preprint. Discussion started: 13 June 2025

1b. Further, the region situated 130m from the landslide origin was considered a stable region, as the maximum runout length of a landslide in this region is approximately 130m. Consequently, the non-hazardous cells within these stable zones hold significant importance in any probabilistic model (Giarola et al., 2024).

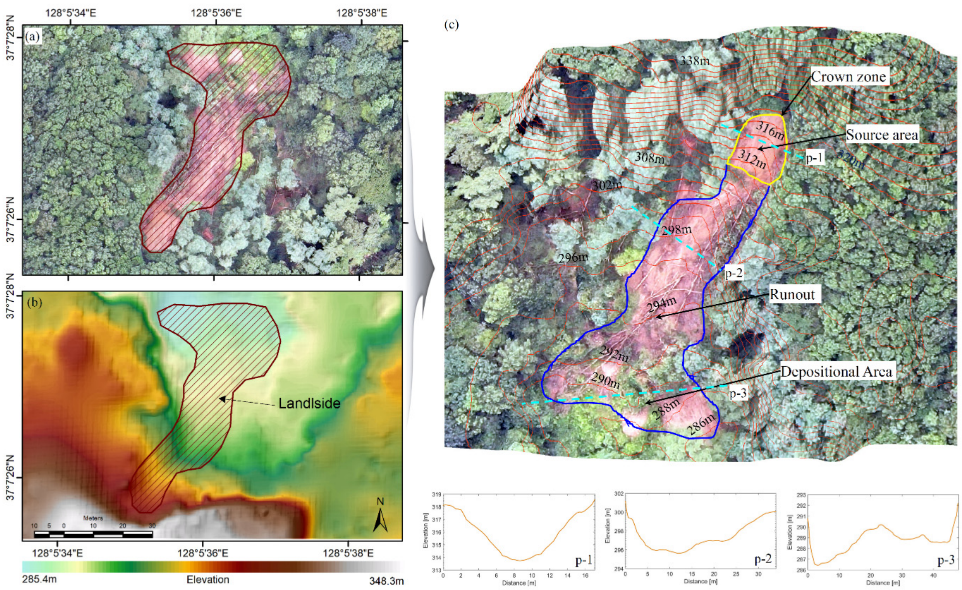

Fig. 4 **a** dronograph of a shallow landslide captured during the field investigation, **b** high-resolution DEM constructed from drone orthophotos, and **c** landslide source and runout area marked in yellow and blue color, respectively. The subplots (**p-1** to **p-3**) represent the crossectional elevation profile of the source, runout and accumulation areas (marked in Fig. 4c).

3.1.2. Predisposing factors

Rainfall-induced landslides in mountainous regions are quite frequent. In order to accurately assess landslide hazards, a deep understanding of the landslide characteristics and its mechanics is often necessary. Several factors influence the initiation of debris flows, including topography, hydrology, lithology, soil and forest (Table 1). The relevant topographic predisposing factors used for the landslide susceptibility model are the slope, aspect, topographic position index (TPI), convergence index (CI), topographic roughness index (TRI), plan curvature, profile curvature, and landforms. The significant hydrological predisposing factors include slope length (SL), stream power index (SPI) and topographic wetness index (TWI) that characterize debris material's concentration, dispersion, and balance on slopes. In

https://doi.org/10.5194/egusphere-2025-1169
Preprint. Discussion started: 13 June 2025

addition, soil (i.e., soil texture, soil thickness), lithology (i.e., surface lithology, average shear-wave velocity), and timber factors (i.e., timber density, diameter and ages) influence the geographic distribution of landslide events. The topographic and hydrologic predisposing factors were generated from a high-resolution DEM (5 × 5 m grid) using ArcGIS, QGIS and SAGA GIS software. The soil, lithology, and timber factors were extracted from the digital soil, geology, and forest database. On the other hand, the velocity-slope model proposed by Wald and Allen (Wald and Allen, 2007) was used to generate the subsurface properties of rock and soil. Subsequently, we considered 18 predisposing factors for landslide susceptibility analysis of the Jecheon-si region.

Table 1 Description of landslide predisposing factors.

Data	Factors	Data Types	Scale	Sources
Topographic Factors	Slope	GRID	1:5000	National Geographic Information Institute (NGII)
	Aspect			
	plan curvature			
	profile curvature			
	topographic position index (TPI)			
	convergence index (CI)			
	topographic roughness index (TRI)			
	landforms			
Hydrological Factors	slope length (SL)	GRID	1:5000	NGII
	topographic wetness index (TWI)			
	stream power index (SPI)			
Forest Factors	Timber Density	Polygon	1:25000	The forest map produced by Korea Forest Service (KFS)
	Timber Diameter			
	Timber Age			
Soil Factors	Soil Types	Polygon	1:25000	The detailed soil map produced by the Rural Development Administration (RDA)
	Soil Thickness			
Surface and sub-subsurface geology Factors	Surface Geology	Polygon	1:50000	Korean Institute of Geoscience and Mineral Resources (KIGAM)
	Time average shear-wave velocity (V_s^{30})	GRID	1:5000	NGII
Rainfall	Daily Rainfall data	Observations	-	KMA (https://data.kma.go.kr/c)

3.1.2.1 Topographic factors

Landform and topography are crucial in the formation of landslides. The Korean National Geographic Information Institute (NGII) provided a high-resolution (5m×5m) digital elevation model (DEM). After that, the pertinent topographic predisposing factors, i.e., slope,

https://doi.org/10.5194/egusphere-2025-1169
Preprint. Discussion started: 13 June 2025

aspect, TPI, CI, plan curvature, profile curvature, TRI, and landforms, were derived from DEM for susceptibility modeling.

The slope is a crucial indicator of the landslide process and is used in almost all landslide susceptibility studies (Fadhillah et al., 2022). The slope's gravitational potential energy is greater at higher elevations than at lower elevations. Generally, landslides occur more frequently on steeper slopes (> 25°) than on flatter slopes (Lee and Min, 2001). Consequently, the slope angle affects the weak rock and soil strata on the slope in terms of their strength and movement rate. Slope stability generally decreases with increasing slope angle. The slope angle of the Jecheon-si region ranges from 0 to 76°, as shown in Fig. 5a.

The topographic aspect controls the movement of water flow, vegetation and sun radiation, which influence landslide behaviors and types (Panahi et al., 2020). It represents the highest downhill slope. Additionally, slopes that face north or east are more likely to experience landslides due to increased exposure to moisture from prevailing winds. The topographic aspect value was classified into nine categories, as presented in Fig. 5b.

Slope instability is influenced by curvature, representing slope variations over a curve's tiny arcs. The plan and profile curvature of the Jecheon-si region ranges from -50.57 to 26.47 and -47.26 to 50.98, respectively, as shown in Figs. 5c & d. In general, convex surfaces are typically represented by positive curvature values, while concave surfaces are indicated by negative curvature values (Lee and Min, 2001). Negative curvature values have a higher likelihood of triggering landslides. On the other hand, Profile curvature describes the direction of the maximum slope and affects flow (convergence and divergence) across the surface (Oh and Lee, 2017).

The convergence index (CI) is an essential topographic predisposing factor for landslide susceptibility analysis. The CI of the Jecheon-si region ranges from -24.58 to 22.57, as shown in Fig. 5(e). The positive values of the convergence index represent ridges, whereas negative ones represent regional depressions (Petschko et al., 2014). In addition, the secondary geo-morphometric parameters, known as the terrain roughness index (TRI), characterize the local relief (Saha et al., 2021). The TRI determines the local terrain's roughness, which influences topographic and hydrological processes critical for developing landslides. Furthermore, the TRI also describes the state of drainage flow in a given area, which helps identify potential landslides. The TRI of the Jecheon-si region ranges from 0 to 14, as depicted in Fig. 5f.

The TPI is a numerical measure of a given location's relative elevation compared to its surrounding area. It represents the terrain's erosion/accumulation capacity (Park et al., 2019).

https://doi.org/10.5194/egusphere-2025-1169
Preprint. Discussion started: 13 June 2025

The negative TPI values signified lower elevated features than the surrounding features, and values close to zero are represented as flat areas. In comparison, the positive values indicated typically higher elevated features (Kadavi et al., 2019). The spatial value of TPI varies between -25.7 and 29.6, as depicted in Fig. 5g.

The morphological setting of the area, crucial in regulating and expressing morphodynamic activity, is directly distinguished by the landform classification (Martinello et al., 2022). Therefore, the landform classification was performed using high-resolution DEM data. The entire region was classified into ten landform classes, i.e., high ridges, local ridges, mid-slope drainages, mid-slope ridges, plains, streams, upland drainages, open slopes, upper slopes and valleys (Fig. 5h).

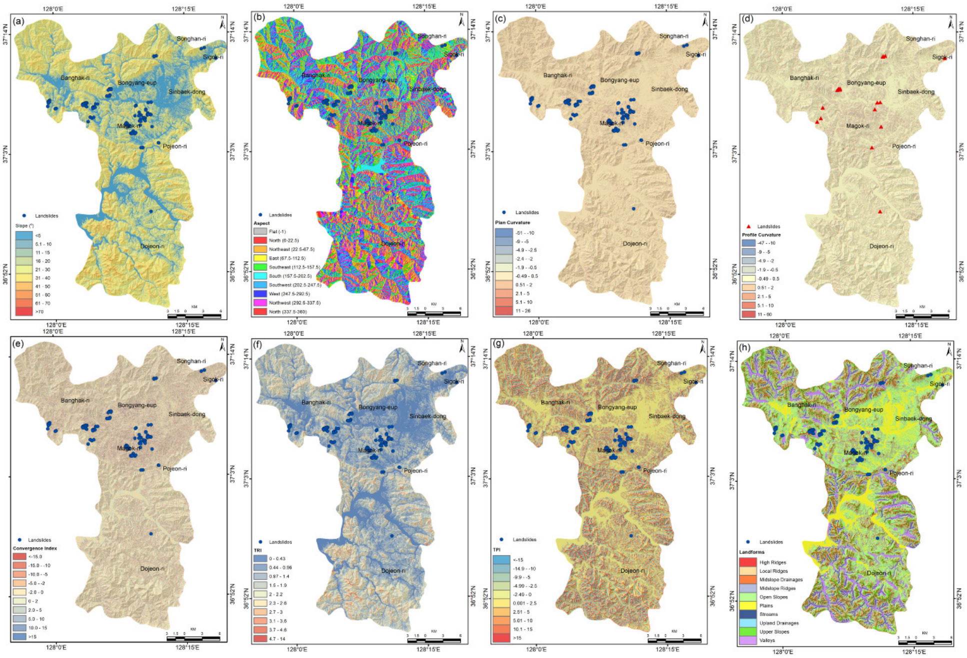

Fig. 5 Topographical predisposing factors of Jecheon-si region.

3.1.2.2 Hydrological factors

The SL, TWI, and SPI are hydrological factors used for the susceptibility analysis. Slope length (SL) is the most critical hydrologic predisposing factor that significantly impacts landslide likelihood. Generally, the distance from the slope's crest to its toe is known as the slope length. The SL is intimately associated with the development of landslides due to the downhill movements of slope materials increasing with the slope length. Thus, the size of the

https://doi.org/10.5194/egusphere-2025-1169
Preprint. Discussion started: 13 June 2025

debris grows with a longer slope length (Qiu et al., 2018). The SL of the Jecheon-si region varies from 0.0 to 423.5, as depicted in Fig. 6a.

The TWI evaluates the topographic effects of hydrological processes by considering slope and flow direction (Panahi et al., 2020). It affects landslide occurrences in mountainous regions (Sameen et al., 2020). The spatial value of TWI varies between 1.98 and 23.3, as shown in Fig. 6b.

The SPI is characterized as the motion of granular material caused by gravity and the erosive power of flowing water (Sameen et al., 2020). It describes the likelihood of flow erosion at a specific point on the topographic surface. The spatial distribution of SPI of the Jecheon-si region varies between 0.68 and 25.41, as depicted in Fig. 6c. Higher SL, SPI, and TWI values indicate greater landslide susceptibility (Sameen et al., 2020; Qiu et al., 2018).

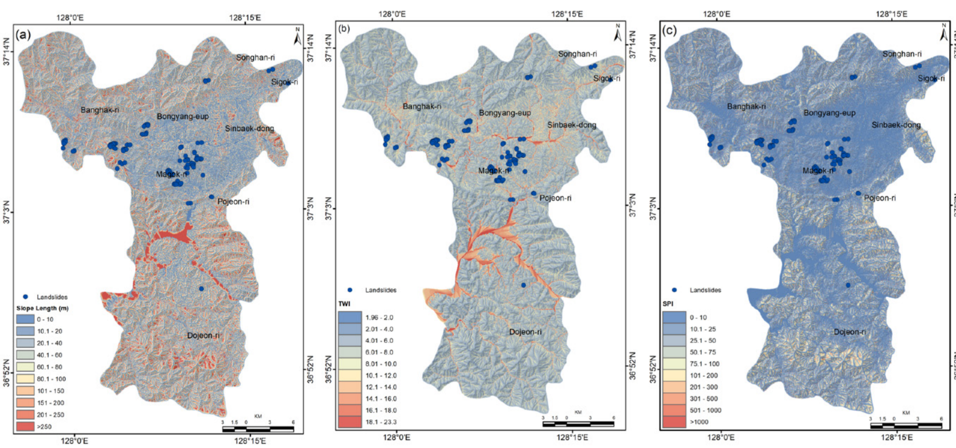

Fig. 6 Hydrological predisposing factors of Jecheon-si region: **a** slope length (SL), **b** topographic wetness index (TWI), and **c** stream power index (SPI).

3.1.2.3 Lithological factors

Outcropping lithology is the most important predisposing factor for landslide evaluation, which is regarded as a good representation of rocks' physical-mechanical characteristics (Lee and Min, 2001). The type and shape of mass movement are mostly controlled by surface geology (Petschko et al., 2014). Furthermore, the occurrence of landslides and their mechanisms could be predicted directly by the geological structure and subsurface rock and soil properties (Panahi et al., 2020). Lithologically, landslides commonly occur in weak rock layers and soft structural planes (Lee and Min, 2001). The outcropping lithology

https://doi.org/10.5194/egusphere-2025-1169
Preprint. Discussion started: 13 June 2025

layers of the Jecheon-si region are shown in Fig. 7a. Most of the study region was covered by granitic rocks (syenite, hornblende, gabbro, diorite, etc.) and metamorphic rocks (phyllite, gneiss, quartzites, etc.) (Jung et al., 2014).

Further, to understand the subsurface properties of rock and soil, a geotechnical site classification in compliance with the NEHRP nomenclature using effective shear-wave velocity (V_s^{30}) based on the topographic gradient (Wald and Allen, 2007) was performed. Figure 7b depicts the seismic site classification of the Jecheon-si region, which exhibits the following site classes: B+ (V_s^{30}: >760 m/s), C (V_s^{30}: 360-760 m/s), D (V_s^{30}:180-360 m/s) and E (V_s^{30}: <180 m/s). The shear-wave velocity reflects the strength and impedance contrast between the various soil/rock layers (Wald and Allen, 2007). Site classes E and D are associated with stiff soils and the soft clay layer, whereas site class B is associated with hard and compact rock. Thus, the average shear-wave velocity is extremely significant in identifying the potential landslide zones (Abd El-Raouf et al., 2021).

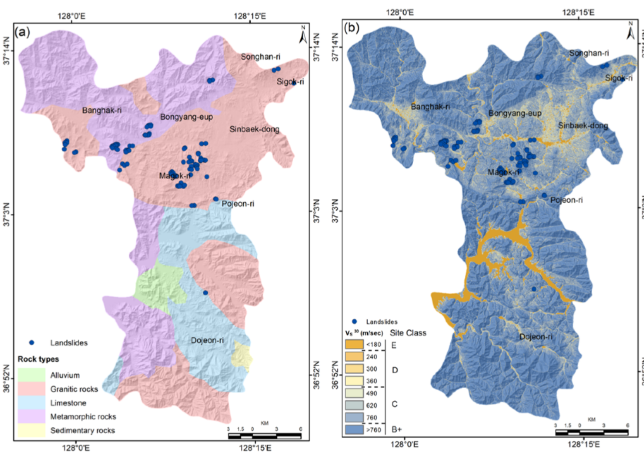

Fig. 7 Lithological predisposing factors of the Jecheon-si region: **a** surface lithology, and **b** average shear-wave velocity (V_s^{30}).

3.1.2.4 Soil factors

A soil's permeability and porosity relate to the soil material, influencing the fluid flow of the region (Lee and Min, 2001). On the other hand, the amount of runoff and the soil's capacity to absorb water is influenced by the soil's thickness (Sameen et al., 2010). Thus, the thickness and texture of the soil are crucial factors in landslide susceptibility assessments. The soil parameters have been extracted from a soil map developed by the Korea Rural Development Administration (KRDA) and used as landslide predisposing factors. Soil texture

https://doi.org/10.5194/egusphere-2025-1169
Preprint. Discussion started: 13 June 2025

of the study region included eight classes: sandy clay loam, sandy loam, loam, silt loam, silty clay, silty clay loam, and silty, as depicted in Fig. 8a. Various studies have shown that sandy and clayey soil is more erosion-resistant than soil with a high silt concentration (Fonseca et al., 2017). On the contrary, soil depth influences the shear stress and shear strength of rock and soil on a slope (Pradhan and Kim, 2014). The depth of the soil also influences the volume of the landslide. The soil thickness of the Jecheon-si region was divided into four classes: very shallow (<20cm), shallow (20–50cm), moderate (50–100cm), and deep (>100cm), as shown in Fig. 8b.

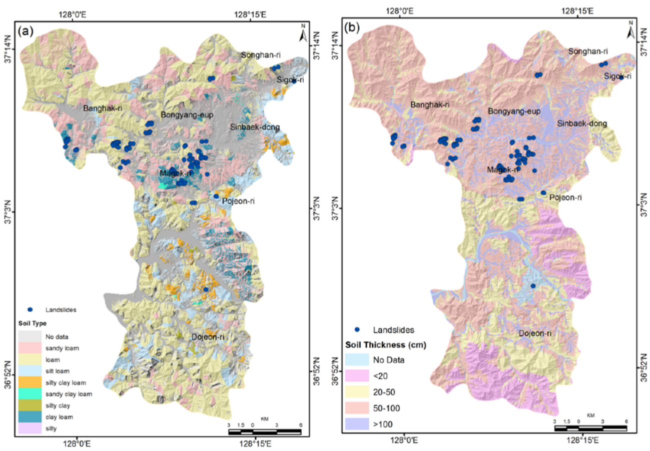

Fig. 8 Soil predisposing factors of Jecheon-si region: **a** soil types and **b** soil thickness.

3.1.2.5 Forest factors

Forest characteristics such as density, diameter, and age are important attributes for landslide susceptibility modeling (Fadhillah et al., 2022). The timber parameters were extracted from the Korea Forest Research Institute and used as landslide predisposing factors. The strength of soil-root connections significantly influences landslides (Kadavi et al., 2019). Thus, forests with medium to large soil-holding capacities have the lowest probability of landslides than non-forest regions (Lee et al., 2004).

The timber diameter was classified into three sizes: large (>30 cm), medium (18-30 cm), and small (<18 cm), as shown in Fig. 9a. The root system's density, which supports and stabilizes the soil, is correlated with the density of the forest (Sameen et al., 2020). For example, an area with dense vegetation can provide stability to keep the soil in place, while an area with sparse vegetation may increase the chances of landslides. The timber density of the Jecheon-si

https://doi.org/10.5194/egusphere-2025-1169
Preprint. Discussion started: 13 June 2025

region was divided into three classes: dense, moderate, and loose, as depicted in Fig. 9b. On the other hand, it was reported that the likelihood of a landslide occurring is higher in newly grown trees and less in older ones since aged trees have more roots (Lee and Min, 2001; Oh et al., 2018). Thus, forest age was classified into seven classes: 61-70 years, 51-60 years, 41-50 years, 31-40 years, 21-30 years, 11-20 years, and <10 years, as depicted in Fig. 9c.

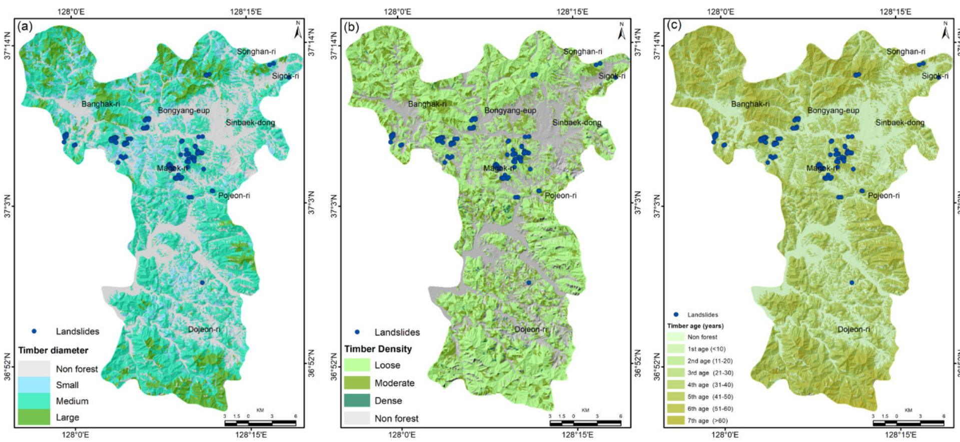

Fig. 9 Forest predisposing factors of Jecheon-si region: **a** timber diameter, **b** timber density, and **c** timber age.

3.2 Methodology

Landslide susceptibility was modeled using four statistical models: FR, IV, CF, and LR. Four major steps were followed to achieve this goal: (a) a landslide inventory database was generated to formulate and verify the required maps, (b) a GIS-based raster and vector database of 18 predisposing factors were prepared to calculate the FR, IV, and CF values and to perform subsequent analysis, (c) LR analysis was performed based on the dependent (landslide inventory data) and independent variables (18 predisposing factors), and (d) calculated LSIs were validated using AUC and other statistical methods. This study aims to compare the most widely used landslide susceptibility approaches and gain insight into their precision in prediction capacities in susceptible zones.

3.2.1 Frequency Ratio (FR) model

The FR technique was proposed by Lee and Talib (2005) to explain the connection between landslide locations and predisposing factors. The FR model estimates the probability of an event or phenomenon occurring in a particular area (Lee and Pradhan, 2007). Since the

https://doi.org/10.5194/egusphere-2025-1169
Preprint. Discussion started: 13 June 2025

FR value represents the chance of occurrence, a higher value suggests a higher likelihood of a landslide occurring and a greater associated risk. This method refers to the likelihood of an incident based on data from previous landslides (Yilmaz, 2009). Subsequently, numerous researchers (Agrawal and Dixit, 2022; Sonker et al., 2022; Dash et al., 2022; Huang et al., 2020; Park et al., 2013; Choi et al., 2012; Yilmaz, 2009) round the world frequently used the FR model in landslide susceptibility modeling.

The landslide density in each subclass/attributes layer of the predisposing factor was calculated using Eq. (1) (Dash et al., 2022; Yilmaz, 2009):

$$FR_{ij} = {}^{NL_{ij}/NL_i}\big/_{N_{ij}/N_i} \qquad (1)$$

where FR_{ij} represents the FR value of the j^th^ attribute class in the i^th^ predisposing factor, NL_{ij} represents landslides in the j^th^ attribute class, NL_i represents landslides in the i^th^ predisposing factor (i.e., total landslides), N_{ij} denotes the cells in j^th^ attribute class, and N_i denotes the cells in the i^th^ predisposing factor (i.e., total cells). The conditional probability principle supports the FR approach. There were two possibilities: FR> 1 and FR <1 exhibiting high and weak correlation, respectively (Huang et al., 2020). After that, the probability density (FRP_{ij}) of the j^th^ class of i^th^ predisposing factor was calculated using Eq. (2) (Sonker et al., 2022):

$$FRP_{ij} = {}^{FR_{ij}}\big/_{\sum_{i=1}^{n} FR_{ij}} \qquad (2)$$

Finally, LSI was determined by summing all the FRP_{ij} values based on the following equation:

$$LSI_{FR} = \sum_{i=1}^{n} FRP_{ij} \qquad (3)$$

where LSI_{FR} represents the predicted LSI for each cell. The greater LSI_{FR} value represents the higher chances of landslide occurrence (Dash et al., 2022).

3.2.2 Information Value (IV) model

The IV model calculates the likelihood of a landslide in a specific location (Achu et al., 2022; Zêzere et al., 2017). The model assigns a numerical value to each factor to determine the overall risk of a landslide occurring. The model can identify areas that are most at risk of landslides, allowing for implementing targeted mitigation measures to reduce the risk of landslides. In general, the effect of various predisposing factors on the stability of LSI is represented by information value (Huang et al., 2020). Yin and Yan (1988) first proposed this model for landslide susceptibility analysis. Subsequently, various researchers (Dash et al., 2022; Wang et al., 2019; Chen et al., 2014; Sarkar et al., 2013) used the IV model to map landslide potential zones. The calculated information value determines the landslide occurrence of each attribute class. The percentage of the total number of landslides for each element was considered for computing IV values.

$$IV_{ij} = \ln\left(\frac{Denclass}{Denmap}\right) = ln\left(\frac{NL_{ij}/N_{ij}}{NL_i/N_i}\right) \tag{4}$$

where IV_{ij} represents the information value of the j^th attribute class in the i^th predisposing factor, Denclass represents the landslide density of the j^th attribute class, and Densmap represents the landslide density of the i^th predisposing factor. A positive IV value shows a high correlation between the variable and the landslides. The zero IV shows no relationship between the landslides and class attributes of predisposing factors, while a negative IV suggests a negative relationship, i.e., variables favor slope stability (Chen et al., 2014). The LSI was determined by adding the IV values for each predisposing attribute class as described below,

$$LSI_{IV} = \sum_{i=1}^{n} ln\left(\frac{NL_{ij}/N_{ij}}{NL_i/N_i}\right) \tag{5}$$

The IV for each attribute class of influencing factor was determined based on the existence of landslides in a certain class of influencing factor. Landslides are more likely to occur when IV is high.

3.2.3 Certainty Factor (CF) model

The CF model describes the likelihood of a landslide occurring as related to the amount of energy available to drive the landslide. The model considers various factors that influence the energy available, such as lithological, soil, hydrological, topographical, and forest characteristics. The model then uses these inputs to determine the likelihood of a landslide occurring in a given area (Dash et al., 2022; Wang et al., 2019; Chen et al., 2019, Devkota et al., 2013). The CF model is commonly used to assess unstable areas that have not experienced landslides and the potential for further landslides in regions that have already experienced it (Wang et al., 2019). The CF value was determined using Eq. (6) (Dash et al., 2022; Devkota et al., 2013):

$$CF_{ij} = \begin{cases} \frac{pp_{ij}-pp_i}{pp_{ij}(1-pp_i)} pp_{ij} \geq pp_i \\ \frac{pp_{ij}-pp_i}{pp_i(1-pp_{ij})} pp_{ij} < pp_i \end{cases} \tag{6}$$

where pp_{ij} is the conditional probability in j^th attribute class of i^th predisposing factor and is expressed as follows:

https://doi.org/10.5194/egusphere-2025-1169
Preprint. Discussion started: 13 June 2025

$$pp_{ij} = \frac{NL_{ij}}{N_{ij}} \quad (7)$$

$$pp_i = \frac{NL_i}{N_i} \quad (8)$$

The CF value ranges from -1 to 1. A higher chance of landslides is indicated by a positive CF value, while a low likelihood is characterized by a negative CF value (Wang et al., 2019). The CF value near zero does not indicate the certainty of landslide activities (Dash et al., 2022). The LSI was calculated based on adding CF values of all predisposing factors using Eq. (9).

$$\mathrm{LSI}_{CF} = \sum CF_{ij} \quad (9)$$

Generally, the high value of LSI_{CF} represents greater chances of landslide susceptibility.

3.2.4 Multivariate Logistic Regression (LR) model

The LR model performs multivariate correlation analysis to investigate the connection between independent and dependent variables. It is used to determine the probability of an outcome based on various predictor variables (Devkota et al., 2013). A multivariate logistic regression determines the proportional contribution of each independent variable to a dependent variable's probability (Choi et al., 2012). It is used to determine the impact of several independent variables on the likelihood of an event occurring. LR model is the most common and reliable approach frequently used to evaluate the relationship between landslide inventory and predisposing factors (Zhou et al., 2021; Aditian et al., 2018; Park et al., 2013; Yilmaz, 2009). Lee (2005) outlines the connection between the predisposition factors and the occurrence of the phenomenon as,

$$P = \frac{1}{1+e^{-Z}} \quad (10)$$

where z is a linear combination of predisposing factors (i.e., independent variables) and p denotes the likelihood of a landslide occurring. In an S-shaped curve, the probability varies from 0 to 1. Equation (11) represents the linear combination of predisposing factors.

$$\mathrm{Z} = \beta_0 + \beta_1 x_1 + \beta_2 x_2 + \beta_3 x_3 + \cdots + \beta_n x_n \quad (11)$$

where β_0 and β_i represent the linear model's constant and regression coefficients, while x_i represents the individual predisposing factor. The coefficient of each landslide predisposing factor was determined using MATLAB. After that, the likelihood of landslides occurring for each pixel was estimated using ArcGIS software based on the coefficient values.

3.2.5 Model performance

Model validation refers to evaluating a model's accuracy and reliability, typically by comparing the model's predictions with in-situ observations. It can help identify any errors or

https://doi.org/10.5194/egusphere-2025-1169
Preprint. Discussion started: 13 June 2025

biases in the model and determine the extent to which it can accurately predict the outcome of interest. In this paper, landslide density (Li), precision (P), MAE, MSE, RMSE, R-index, and AUC were utilized to assess the effectiveness of the LSI models (He et al., 2021; Mandal et al., 2021; Chen et al., 2019). The model validation was performed by examining the relationship between the inventory and landslide susceptibility zones based on the R-index analysis. The R-index was determined by applying Eq. (12) (Trinh et al., 2022; Shahabi and Hashim, 2015):

$$R = ({}^{n_i}/_{N_i}) / \Sigma({}^{n_i}/_{N_i}) \times 100 \tag{12}$$

where n_i represents the landslide inventory in the LSI zone, while N_i represents the pixels in the same LSI zone. On the other hand, the precision (P) parameter is widely used to validate the predicted LSI. Thus, the precision of the predicted LSI was determined using Eq. (13) (Ayalew et al., 2005).

$$p = L_{hs}/L_T \tag{13}$$

L_{hs} represents the landslides in the severe to high LSI zone, while L_T represents all landslides in the region.

The MAE, MSE, and RMSE were also used to analyze the effectiveness of the LSI model (Mandal et al., 2021; He et al., 2021; Chen et al., 2019). The RMSE and MSE measure the forecasting errors of the model, whereas the MAE measures its generalization error (Mandal et al., 2021). The RMSE, MAE, and MSE were determined using the following Eqs. (14-16):

$$RMSE = \sqrt{\frac{1}{n}\sum_{i=1}^{n}(l_{obs} - l_{pre})^2} \tag{14}$$

$$MAE = \frac{1}{n}\sum_{i=n}^{n}\left|(l_{obs} - l_{pre})\right| \tag{15}$$

$$MSE = \frac{1}{n}\sum_{i=n}^{n}(l_{obs} - l_{pre})^2 \tag{16}$$

where l_{obs} denote the observed landslides, l_{pre} is the calculated LSI values, and n represents the inventory dataset (total samples) (He et al., 2021). A lower RMSE value denotes better model performance.

Moreover, another common and widely adopted method frequently utilized to assess the model performance in landslide susceptibility analysis is the Area Under the Receiver Operating Characteristic Curve (AUC) (He et al., 2021, Pham et al., 2020). AUC measures how accurately a predictive model can classify data points. Generally, the AUC curves are used to calculate the precision of absence or presence prediction models (Shirzadi et al., 2017).

https://doi.org/10.5194/egusphere-2025-1169
Preprint. Discussion started: 13 June 2025

Higher AUC values indicate better performance, with a range of 0.5 to 1 (Chen et al., 2019; Shahabi and Hashim, 2015).

4. Results and Discussion

4.1 The spatial relationship between the predisposing factors and landslide inventory

The landslide susceptibility of the Jecheon-si region was investigated using the FR, IV, CF, and LR methods based on the landslide inventory data and 18 landslide influencing factors. The relationship between the influencing factors viz. topographic slope, aspect, landforms class, average shear-wave velocity, TPI, CI, TWI, TRI, plan curvature, profile curvature, SPI, SL, surface lithology, soil thickness, timber density, timber age, soil type, timber diameter and the landslide inventory locations were performed. After that, a spatial database was constructed with a 5×5 m grid size. A relationship between the predisposing factors and landslide inventory is depicted in Fig. 10 and Table 2.

Table 2 Spatial relationships between landslide inventory location and the predisposing factors.

Predisposing Factors	Attributes	Area (km^2)	% of A	landslides	% of L	FRP_{ij}	IV_{ij}	CF_{ij}
Landforms	Streams	30.85	3.49	0	0.00	0.00	0.000	-1.000
	Midslope Drainages	78.29	8.85	12	10.71	0.12	0.083	0.174
	Upland Drainages	10.06	1.14	4	3.57	0.32	0.497	0.681
	Valleys	79.67	9.01	1	0.89	0.01	-1.004	-0.901
	Plains	102.69	11.61	0	0.00	0.00	0.000	-1.000
	Open Slopes	377.34	42.67	58	51.79	0.12	0.084	0.176
	Upper Slopes	70.01	7.92	12	10.71	0.14	0.131	0.261
	Local Ridges	2.80	0.32	0	0.00	0.00	0.000	-1.000
	Midslope Ridges	76.62	8.66	16	14.29	0.17	0.217	0.394
	High Ridges	56.00	6.33	9	8.04	0.13	0.103	0.212
V_s^{30} (m/sec)	<180	45.58	5.16	0	0.00	0.00	0.000	-1.000
	180-240	0.06	0.01	0	0.00	0.00	0.000	-1.000
	240-300	0.03	0.00	0	0.00	0.00	0.000	-1.000
	300-360	6.46	0.73	0	0.00	0.00	0.000	-1.000
	360-490	27.78	3.14	0	0.00	0.00	0.000	-1.000
	490-620	89.10	10.08	0	0.00	0.00	0.000	-1.000
	620-760	254.68	28.82	35	31.25	0.45	0.035	0.078
	>760	459.87	52.05	77	68.75	0.55	0.121	0.243
Rock Types	Metamorphic rocks	295.70	33.44	36	32.14	0.39	-0.017	-0.040
	Limestone	147.01	16.62	1	0.89	0.02	-1.270	-0.946
	Granitic rocks	407.68	46.10	75	66.96	0.59	0.162	0.312
	Alluvium	27.36	3.09	0	0.00	0.00	0.000	-1.000
	Sedimentary rocks	6.58	0.74	0	0.00	0.00	0.000	-1.000
TRI	0 - 0.43	158.71	17.95	0	0.00	0.00	0.000	-1.000
	0.44 - 0.96	148.21	16.76	6	5.36	0.03	-0.495	-0.680

https://doi.org/10.5194/egusphere-2025-1169
Preprint. Discussion started: 13 June 2025

	0.97 - 1.4	184.18	20.83	21	18.75	0.07	-0.046	-0.100
	1.5 - 1.9	169.91	19.21	27	24.11	0.10	0.099	0.203
	2 - 2.2	112.46	12.72	35	31.25	0.20	0.390	0.593
	2.3 - 2.6	64.51	7.29	12	10.71	0.12	0.167	0.319
	2.7 - 3	30.65	3.47	8	7.14	0.17	0.314	0.515
	3.1 - 3.6	11.97	1.35	2	1.79	0.11	0.120	0.242
	3.7 - 4.6	3.30	0.37	1	0.89	0.20	0.379	0.582
	4.7 - 14	0.43	0.05	0	0.00	0.00	0.000	-1.000
Plan Curvature	-51 - -10	0.05	0.01	0	0.00	0.00	0.000	-1.000
	-9 - -5	1.88	0.21	1	0.89	0.26	0.624	0.762
	-4.9 - -2.5	17.86	2.02	6	5.36	0.16	0.424	0.623
	-2.4 - -2	13.45	1.52	8	7.14	0.29	0.672	0.787
	-1.9 - -0.5	143.57	16.23	32	28.57	0.11	0.245	0.432
	-0.49 - 0.5	509.79	57.65	36	32.14	0.03	-0.254	-0.442
	0.51 - 2	156.94	17.75	22	19.64	0.07	0.044	0.097
	2.1 - 5	38.77	4.38	7	6.25	0.09	0.154	0.299
	5.1 - 10	2.01	0.23	0	0.00	0.00	0.000	-1.000
	11 - 26	0.02	0.00	0	0.00	0.00	0.000	-1.000
Profile Curvature	-47 - -10	0.19	0.02	0	0.00	0.00	0.000	-1.000
	-9 - -5	2.93	0.33	0	0.00	0.00	0.000	-1.000
	-4.9 - -2	35.00	3.96	4	3.57	0.16	-0.045	-0.108
	-1.9 - -0.5	131.70	14.89	25	22.32	0.27	0.176	0.333
	-0.49 - 0.5	507.89	57.43	49	43.75	0.13	-0.118	-0.238
	0.51 - 2	169.50	19.17	29	25.89	0.24	0.131	0.260
	2.1 - 5	34.95	3.95	5	4.46	0.20	0.053	0.115
	5.1 - 10	1.99	0.23	0	0.00	0.00	0.000	-1.000
	10.1 - 60	0.18	0.02	0	0.00	0.00	0.000	-1.000
Slope (degree)	<5	124.19	14.04	0	0.00	0.00	0.000	-1.000
	5-10	71.44	8.08	2	1.79	0.04	-0.656	-0.779
	10-15	81.02	9.16	1	0.89	0.02	-1.011	-0.903
	15-20	104.14	11.78	6	5.36	0.07	-0.342	-0.545
	20-30	270.73	30.61	44	39.29	0.21	0.108	0.221
	30-40	192.86	21.81	49	43.75	0.33	0.302	0.502
	40-50	37.47	4.24	10	8.93	0.34	0.324	0.525
	50-60	2.39	0.27	0	0.00	0.00	0.000	-1.000
	60-70	0.08	0.01	0	0.00	0.00	0.000	-1.000
	>70	0.01	0.00	0	0.00	0.00	0.000	-1.000
Aspect	Flat (-1)	3.60	0.41	0	0.00	0.00	0.000	-1.000
	North (0-22.5)	51.16	5.79	2	1.79	0.04	-0.511	-0.691
	Northeast (22.5-67.5)	107.14	12.12	3	2.68	0.03	-0.655	-0.779
	East (67.5-112.5)	106.91	12.09	22	19.64	0.20	0.211	0.385
	Southeast (112.5-157.5)	107.41	12.15	40	35.71	0.35	0.468	0.660
	South (157.5-202.5)	117.67	13.31	29	25.89	0.23	0.289	0.486
	Southwest (202.5-247.5)	115.99	13.12	8	7.14	0.07	-0.264	-0.455
	West (247.5-292.5)	114.44	12.94	5	4.46	0.04	-0.462	-0.655
	Northwest (292.5-337.5)	108.20	12.24	1	0.89	0.01	-1.137	-0.927
	North (337.5-360)	51.80	5.86	2	1.79	0.04	-0.516	-0.695
SPI	0 - 10	373.32	42.22	33	29.46	0.07	-0.156	-0.302
	10.1 - 25	199.70	22.58	29	25.89	0.12	0.059	0.128
	25.1 - 50	154.83	17.51	30	26.79	0.16	0.185	0.346
	50.1 - 75	64.28	7.27	12	10.71	0.15	0.168	0.322
	75.1 - 100	28.55	3.23	1	0.89	0.03	-0.558	-0.723
	101 - 200	29.73	3.36	4	3.57	0.11	0.026	0.059
	201 - 300	7.37	0.83	1	0.89	0.11	0.030	0.067
	301 - 500	6.66	0.75	2	1.79	0.25	0.375	0.578

https://doi.org/10.5194/egusphere-2025-1169
Preprint. Discussion started: 13 June 2025

	501 - 1000	6.88	0.78	0	0.00	0.00	0.000	-1.000
	>1000	13.01	1.47	0	0.00	0.00	0.000	-1.000
Slope Length (m)	0 - 10	167.36	18.92	19	16.96	0.11	-0.047	-0.116
	10.1 - 20	83.19	9.41	13	11.61	0.15	0.091	0.190
	20.1 - 40	164.46	18.60	24	21.43	0.14	0.062	0.132
	40.1 - 60	121.18	13.70	22	19.64	0.17	0.156	0.302
	60.1 - 80	86.91	9.83	15	13.39	0.16	0.134	0.266
	80.1 - 100	63.00	7.12	7	6.25	0.11	-0.057	-0.140
	101 - 150	90.90	10.28	9	8.04	0.09	-0.107	-0.218
	151 - 200	43.87	4.96	1	0.89	0.02	-0.745	-0.820
	201 - 250	22.50	2.54	0	0.00	0.00	0.000	-1.000
	>250	40.96	4.63	2	1.79	0.05	-0.414	-0.615
TPI	<-15	26.31	2.97	2	1.79	0.06	-0.222	-0.400
	-14.9 - -10	59.49	6.73	11	9.82	0.14	0.164	0.315
	-9.9 - -5	137.34	15.53	12	10.71	0.07	-0.161	-0.310
	-4.99 - -2.5	111.57	12.62	11	9.82	0.07	-0.109	-0.222
	-2.49 - 0	160.83	18.19	12	10.71	0.06	-0.230	-0.411
	0.001 - 2.5	111.70	12.63	12	10.71	0.08	-0.071	-0.179
	2.51 - 5	69.03	7.81	8	7.14	0.09	-0.039	-0.093
	5.01 - 10	99.88	11.29	24	21.43	0.18	0.278	0.473
	10.1 - 15	60.11	6.80	16	14.29	0.20	0.323	0.524
	>15	48.07	5.44	4	3.57	0.06	-0.182	-0.343
Convergence Index	<-15.0	17.75	2.01	1	0.89	0.05	-0.352	-0.555
	-15.0 - -10	17.48	1.98	3	2.68	0.14	0.132	0.262
	-10.0 - -5	52.22	5.90	16	14.29	0.25	0.384	0.587
	-5.0 - -2	103.86	11.74	15	13.39	0.12	0.057	0.123
	-2.0 - 0	247.22	27.96	29	25.89	0.09	-0.033	-0.080
	0 - 2	248.48	28.10	26	23.21	0.08	-0.083	-0.174
	2.0 - 5	111.27	12.58	15	13.39	0.11	0.027	0.061
	5.0 - 10	53.30	6.03	5	4.46	0.08	-0.130	-0.259
	10.0 - 15	16.56	1.87	2	1.79	0.10	-0.021	-0.049
	>15	16.18	1.83	0	0.00	0.05	0.000	-1.000
	<-15.0	17.75	2.01	1	0.89	0.14	-0.352	-0.555
Soil Type	Sandy loam	132.07	14.95	36	32.14	0.21	0.333	0.535
	Loam	307.98	34.87	46	41.07	0.11	0.072	0.179
	Silt loam	66.65	7.55	2	1.79	0.02	-0.625	-0.763
	Silty clay loam	16.57	1.88	2	1.79	0.09	-0.021	-0.047
	Silty clay	2.17	0.25	0	0.00	0.00	0.000	-1.000
	Sandy clay loam	1.18	0.13	0	0.00	0.00	0.000	-1.000
	Clay loam	26.55	3.01	19	16.96	0.55	0.752	0.823
	Silty	0.07	0.01	0	0.00	0.00	0.000	-1.000
	No data	330.00	37.36	7	6.25	0.02	-0.777	-0.833
Soil Thickness (cm)	<20	89.07	10.07	0	0.00	0.00	0.000	-1.000
	20-50	203.19	22.98	10	8.93	0.13	-0.411	-0.611
	50-100	461.05	52.14	92	82.14	0.53	0.197	0.365
	>100	108.38	12.26	9	8.04	0.22	-0.183	-0.344
	No Data	22.64	2.56	1	0.89	0.12	-0.457	-0.651
Timber Density	Loose	468.53	52.98	86	76.79	0.53	0.161	0.310
	Moderate	143.98	16.28	21	18.75	0.42	0.061	0.132
	Dense	7.24	0.82	0	0.00	0.00	0.000	-1.000
	Non forest	264.59	29.92	5	4.46	0.05	-0.826	-0.851
Timber diameter	Small	418.24	47.36	86	76.79	0.47	0.210	0.383
	Medium	96.33	10.91	18	16.07	0.42	0.168	0.321
	Large	105.18	11.91	3	2.68	0.06	-0.648	-0.775
	Non forest	263.38	29.82	5	4.46	0.04	-0.825	-0.850
Timber age	1st age	0.03	0.00	0	0.00	0.00	0.000	-1.000
	2nd age	14.54	1.65	47	41.96	0.80	1.406	0.961
	3rd age	91.11	10.32	3	2.68	0.01	-0.586	-0.740
	4th age	168.55	19.09	6	5.36	0.01	-0.552	-0.719
	5th age	249.71	28.28	39	34.82	0.04	0.090	0.188
	6th age	84.44	9.56	12	10.71	0.04	0.049	0.108

	7th age	11.39	1.29	5	4.46	0.11	0.539	0.711
	Non forest	263.34	29.82	0	0.00	0.00	0.000	-1.000
TWI	1.96 - 2.0	0.000156	0.000017	0	0	0.00	0.000	-1.000
	2.01 - 4.0	20.82	2.35	4	3.57	0.39	0.181	0.340
	4.01 - 6.0	523.38	59.23	88	78.57	0.34	0.123	0.246
	6.01 - 8.0	187.93	21.27	18	16.07	0.20	-0.122	-0.244
	8.01 - 10.0	58.08	6.57	2	1.78	0.07	-0.566	-0.728
	10.1 - 12.0	26.97	3.05	0	0	0.00	0.000	-1.000
	12.1 - 14.0	24.88	2.81	0	0	0.00	0.000	-1.000
	14.1 - 16.0	19.39	2.19	0	0	0.00	0.000	-1.000
	16.1 - 18.0	12.72	1.44	0	0	0.00	0.000	-1.000
	18.1 - 23.3	9.33	1.05	0	0	0.00	0.000	-1.000

The FR value indicates how closely landslides and a particular factor's attribute are related, i.e., the higher the ratio, the stronger the association. The larger ratio indicated a more significant association between the attribute of the given factor and occurrences of landslides (Lee and Talib, 2005). The FR analysis exhibited that 40°- 50° slope angles have maximum landslide occurrences (FR=2.11). In general, the slope shear stress changes as the slope angle increases, which might result in landslides in a specific range (Chen et al., 2021; Park et al., 2013). The FR analysis confirms the above statements. The other slope ranges, i.e., 5-10° (FR=0.04), 10-15° (FR=0.02), 15-20° (FR=0.07), 20-30° (FR=0.21), and 30-40° (FR=0.33) have decreasing order of the FR as depicted in Fig. 10. The maximum FR value (2.94) in the slope aspect factor was observed in southeast-facing slopes. A landslide is likely also present on the slopes facing east and south (FR = 1.62 and 1.95, respectively). For the other six aspects classes, the FR value varies from 0.07 to 0.54, while zero FR is observed in the flat region. For the plan and profile curvature, the plane curvature class of -2 to -2.5 is associated with a higher FR value (4.70) and is most susceptible to slope failure. On the other hand, the -0.5 to -1.9 class of the profile curvature was associated with higher FR (1.50) and had the highest probability of landslide occurrences. The convergence index presented the higher FR value associated with a subclass ranging from -5 to -10 (FR=2.42). The FR analysis of the landform class showed that the upland drainages were more susceptible to slope failure (FR= 3.14), and local ridges were less vulnerable (FR=0). On the other hand, a high FR value was associated with the TPI class of 10.1-15 (FR=2.10). Regarding the TRI factor, the higher FR value was related to the TRI classes of 1.5 to 4.6, as depicted in Fig. 10.

Figure 10 depicts the correlation between the rate of landslide occurrence and the SPI. It was observed that the SPI subclass of 300-500 was associated with higher FR (2.40) and was most susceptible to slope failure. A higher SPI value often indicates a higher likelihood of a landslide occurring. The TWI subclass of 2.0-4.0 was associated with higher FR (1.46),

https://doi.org/10.5194/egusphere-2025-1169
Preprint. Discussion started: 13 June 2025

representing higher landslide occurrences. For slope length, the higher FR value was observed in the slope length of <100m, while relatively low FR values were associated with higher slope length (Fig. 10). The surface geology showed that granitic and metamorphic rocks with FR values of 1.45 and 0.96 were the rock outcrop most likely to experience landslides. On the other hand, the average shear wave velocity indicates that site class C1 (V_s^{30}~ 620-760 m/sec) and B (V_s^{30} >760 m/sec) are vulnerable to slope failure with FR values of 1.08 and 1.32, respectively.

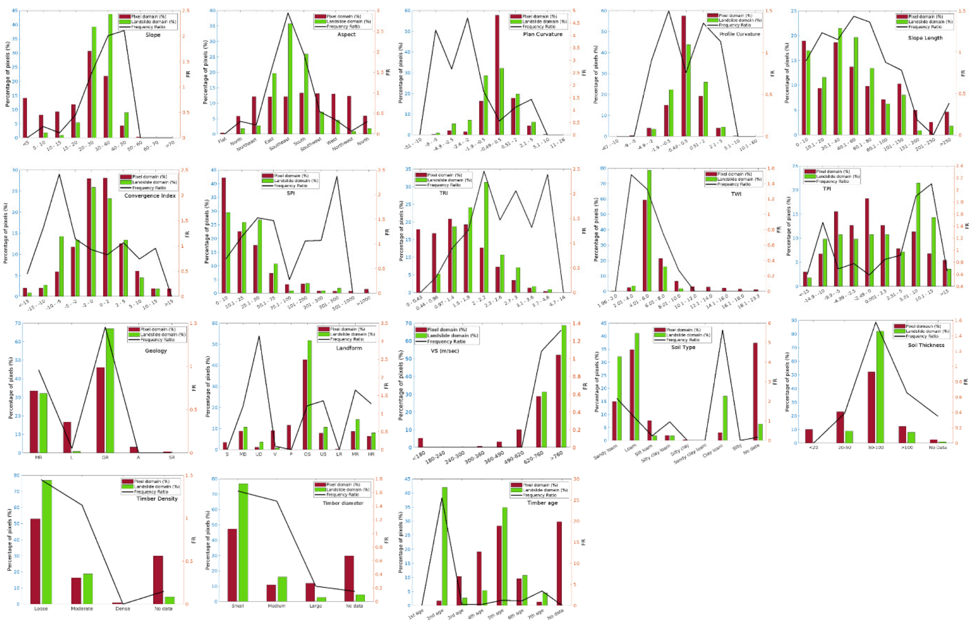

Fig. 10 The spatial relationship between the landslide locations and the predisposing factors.

Regarding the soil, the spatial relationship between the landslide locations and the eight soil types shows a clear difference in relevance to the likelihood of landslides. It was observed that the clay loam soil is most likely to slide (FR= 5.65), while silty clay and sandy clay are relatively stable. On the other hand, soil depth also plays a role in the water content of the soil, as soils with deeper depth can hold more water and become saturated more easily. The higher FR values were observed in the soil depth of >50 cm. The study explored the relationships between timber diameter, density, and age as factors associated with forest type and landslides. The FR was high in low-density forest areas (FR= 1.62). In the case of the timber age class, the FR is higher for 10 to 20-year-old forest areas (FR=0.80). Conversely, small-diameter timber was associated with higher landslide probability (FR= 25.48).

https://doi.org/10.5194/egusphere-2025-1169
Preprint. Discussion started: 13 June 2025

4.2. Multi-collinearity analysis of predisposing factors

The statistical phenomenon of multi-collinearity arises when two or more predictor variables in a regression model are strongly correlated (Zhou et al., 2021). The multi-collinearity of predisposing factors will negatively affect the model's outcomes, reducing its predictive power or perhaps making it fail. Therefore, understanding collinearity among the predisposing factors, that is, whether there is a linear correlation among the independent predisposing factors, is critical before performing the LR modeling. Here, we determined the multi-collinearity among predisposition factors using the variance inflation factor (VIF) and tolerance (Chen and Chen, 2021).

$$TOL = \frac{1}{VIF} \tag{17}$$

$$VIF = \frac{1}{1-{R_i}^2} \tag{18}$$

where R_i^2 represents the coefficient of determination of regression of variable 'i' on all other variables (Hong et al., 2020). Table 3 illustrates the results of the multi-collinearity analysis for all variables that met the threshold values (VIF<10 or tolerance > 0.1) (Zhang et al., 2020; Kadavi et al., 2019). According to the results of the multi-collinearity diagnostics tests (Table 3), TRI has the highest VIF (6.483) and lowest tolerances (0.154), which are far from the critical values. Subsequently, these eighteen variables were selected for LSI modeling.

Table 3 Regression coefficient and collinearity of the landslide-predisposing factors.

Predisposing factors	β	Collinearity statistics	
		Tolerance	VIF
Slope	9.527	0.158	6.341
Aspect	10.547	0.890	1.123
Convergence index	-1.095	0.687	1.455
Plane curvature	3.093	0.607	1.646
Profile curvature	4.089	0.870	1.149
TRI	-4.953	0.154	6.483
TPI	2.679	0.780	1.282
Landform	13.603	0.529	1.890
Slope Length	16.704	0.865	1.157
TWI	-5.004	0.547	1.827
SPI	3.956	0.810	1.235
Geology	6.223	0.897	1.115
V_s^{30}	2.381	0.488	2.049
Soil type	6.696	0.701	1.427
Soil thickness	4.654	0.889	1.125

https://doi.org/10.5194/egusphere-2025-1169
Preprint. Discussion started: 13 June 2025

Timber density	2.897	0.212	4.722
Timber diameter	-0.208	0.278	3.593
Timber age	2.244	0.777	1.287
Intercept	-16.500	-	-

4.3 Landslide susceptibility index (LSI) based on the FR, IV, CF and LR models

The FR, IV, CF and LR models were independently constructed to determine the LSI using Eqs. 3, 5, 9 and 11. Here, we used ArcGIS software to develop the LSIs based on four statistical models. The calculated LSI values for the FR, IV, CF and LR models vary from 0.47 to 6.06, -10.15 to 5.06, -14.56 to 7.66, and 0-1, respectively. High LSI values represent more susceptibility to landslides, whilst low LSI levels suggest less susceptibility to landslides (Dash et al., 2022). The LSI value was then normalized using Eq. (19) to understand the effectiveness of predicted LSI with the topographic and landslide characteristics.

$$LSI_{nm} = \frac{LSI_o - LSI_{\min}}{LSI_{\max} - LSI_{min}} \quad (19)$$

where LSI_{nm} represents the normalized landslide susceptibility index for FR, IV, CF and LR models, LSI_o represents the original LSI value, and LSI_{max} & LSI_{min} represent the minimum and maximum LSI value. The normalized LSI values for the FR, IV, CF, and LR models are depicted in Fig. 11. The spatial distribution of LSI values derived based on the FR, IV, and CF models (Figs. 11a-c) was somewhat comparable. On the other hand, the LSI distribution computed through the LR model differs from the other models (Fig. 11d). The distribution of LSI showed that high-elevation areas have a higher likelihood of experiencing landslides. The region's northern, southern and central parts, with steep slopes surrounding the valley, were identified as the most vulnerable region. On the other hand, relatively flat areas exhibited low landslide potential. It was noted that the majority of the land cover in this region had a low density of forests.

https://doi.org/10.5194/egusphere-2025-1169
Preprint. Discussion started: 13 June 2025

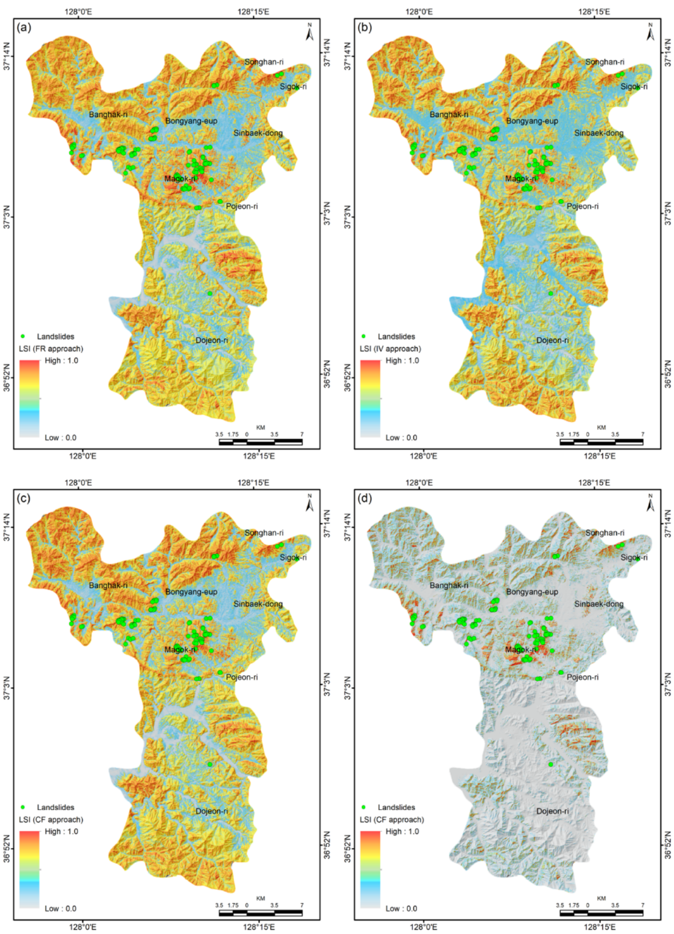

Fig. 11 Landslide susceptibility index of the Jecheon-si region based on the **a** FR, **b** IV, **c** CF, and **d** LR model.

Table 4 illustrates the MSE, RMSE, MAE, and AUC values of the FR, IV, CF and LR models. The AUC values for the FR, IV, CF, and LR models were found to be 0.889, 0.872, 0.877, and 0.912, respectively. All four of the models' AUC values were greater than 0.80, showing that the LSI models had strong prediction abilities. Based on the inventory datasets, the models' accuracy was further examined using RMSE, MSE, and MAE. The outcome demonstrates that the FR, CF and IV models had the lowest RMSE, MSE, and MAE values. On the other hand, the LR model had higher MAE, MSE, and RMSE values, signifying lower prediction accuracy than other models. The LR model, however, performs better than other

https://doi.org/10.5194/egusphere-2025-1169
Preprint. Discussion started: 13 June 2025

models in terms of AUC value. Therefore, selecting an appropriate model for landslide susceptibility mapping is difficult even though the performances and prediction accuracy of all the discussed models were acceptable.

Table 4 Validation of models by AUC, RMSE, MSE, and MAE.

Models	AUC	MAE	MSE	RMSE
FR	0.889	0.281	0.087	0.295
IV	0.872	0.238	0.059	0.243
CF	0.877	0.226	0.064	0.252
LR	0.912	0.272	0.147	0.385

In this study, we used a different method to evaluate the results of LSI. The approach uses a high-resolution DEM, aerial photos, and drone images to determine whether a landslide disaster is likely in the predicted very high susceptibility area (He et al., 2021). We also used the 1D elevation profile to check whether the predicted LSI distribution is consistent with the topographic and landslide characteristics. To better display the experiment and evaluate the model accuracy, we selected recent landslide sites that have never previously experienced landslides. The aerial photo was acquired from the NGII web portal (https://map.ngii.go.kr/) for 2020 to 2021, and the drone survey was conducted in August 2020. Figure 12 depicts the LSI distribution and the landslide area on a dronograph and elevation profile from the landslide source area to the landslide deposition zone. The landslide-affected regions are clearly visible in both the drone and the aerial photos. The predicted LSI value based on the FR, IV, and CF models was found to be very high in both the crown and the landslide deposit zone (Fig. 12f). In contrast, the LSI predicted by the LR model was low in the landslide deposit zone and moderate in the crown zone (Fig. 12f). The four applied models were found to be able to predict the location of the landslide precisely; however, they are not consistent with the landslide and topography characteristics. To overcome this issue, we put forth a hybrid integrated strategy to verify that the LSI derived using an integrated approach is consistent with topography and landslide characteristics.

https://doi.org/10.5194/egusphere-2025-1169
Preprint. Discussion started: 13 June 2025

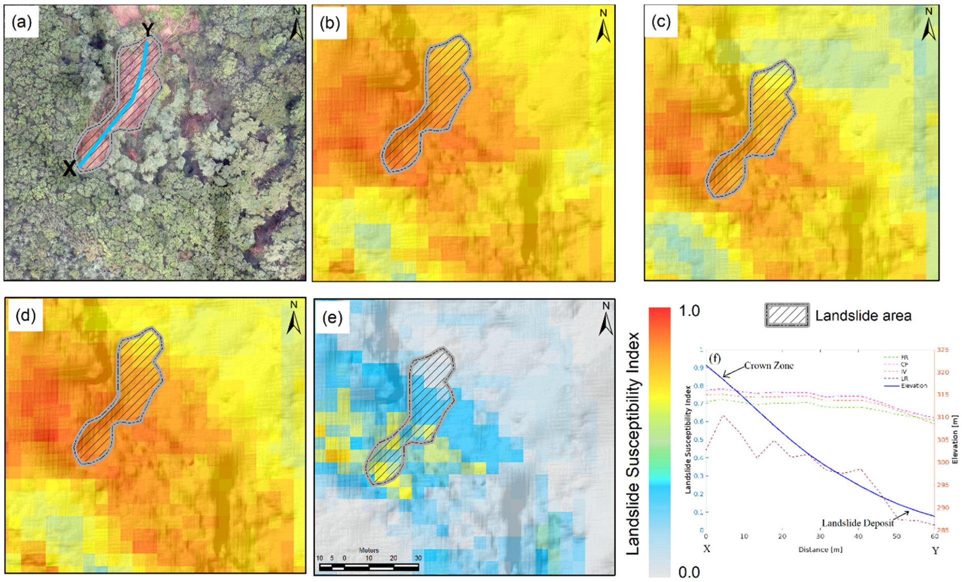

Fig. 12 Spatial characteristics of predicted LSIs: **a** Drone image acquired in August 2020, **b** LSI based on the FR model, **c** LSI based on the IV model, **d** LSI based on the CF model, **e** LSI based on the FR model and **f** elevation profile and LSI distribution from the landslide source area to landslide deposit zone.

4.4 LSI based on a hybrid integrated approach

A combination of different models is one of the options for improving model accuracy. Therefore, we integrated the above four models using Eq. (20).

$$LSI_{intergrated} = w_{0.25}.LSI_{FR}+w_{0.25}.LSI_{IV}+w_{0.25}.LSI_{CF}+w_{0.25}.LSI_{LR} \quad (20)$$

where LSI_{FR}, LSI_{IV}, LSI_{CF}, and LSI_{LR} represent the normalized LSI of each model, and w represents the weight of each LSI model. The spatial distribution of LSI estimated using the integrated technique is shown in Fig. 13. It was observed that the LSI predicted through the integrated approach was consistent with the topographic profile and landslide characteristics, which was not in the earlier case. For example, a high LSI value was observed in the landslide source area, while a low LSI value was observed in the landslide deposit zone (Figs. 13b′-d'). Therefore, the LSI calculated through the hybrid integrated approach was used for further analysis.

https://doi.org/10.5194/egusphere-2025-1169
Preprint. Discussion started: 13 June 2025

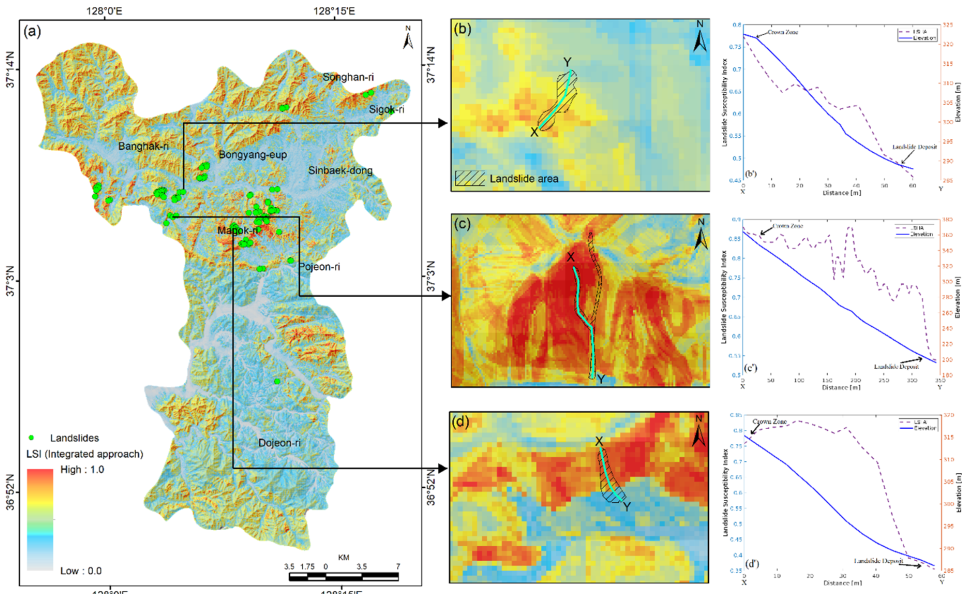

Fig. 13 LSI based on the hybrid integrated approach: **a** spatial distribution of LSI in the Jecheon-si region, **b-d** the details of LSI distribution of three recent past landslide events, and **b'-d'** elevation profile and LSI distribution from the landslide source area to landslide deposit zone at different landslide sites.

The LSI was categorized using Jenks natural breaks (Huang and Zhao, 2018) into five microzones: unlikely, low, moderate, high, and severe. The landslide hazard microzonation map (Fig. 14a) shows that 2.73% of the total areas are classified as severe susceptibility (SS). The areas classified as high, moderate, low, and unlikely zones were 14.94%, 40.31%, 30.20%, and 11.82%, respectively. The severe susceptibility region was observed to contain 41.96% of landslides, while the area of the unlikely zone is associated with zero landslides. A potential landslide-prone area can be seen on the map in the central part of the study area, i.e., the Magok-ri region. The landslide hazard microzonation map derived through the hybrid integrated approach is accurate and relevant since more landslides occur in the zones with the highest susceptibility.

https://doi.org/10.5194/egusphere-2025-1169
Preprint. Discussion started: 13 June 2025

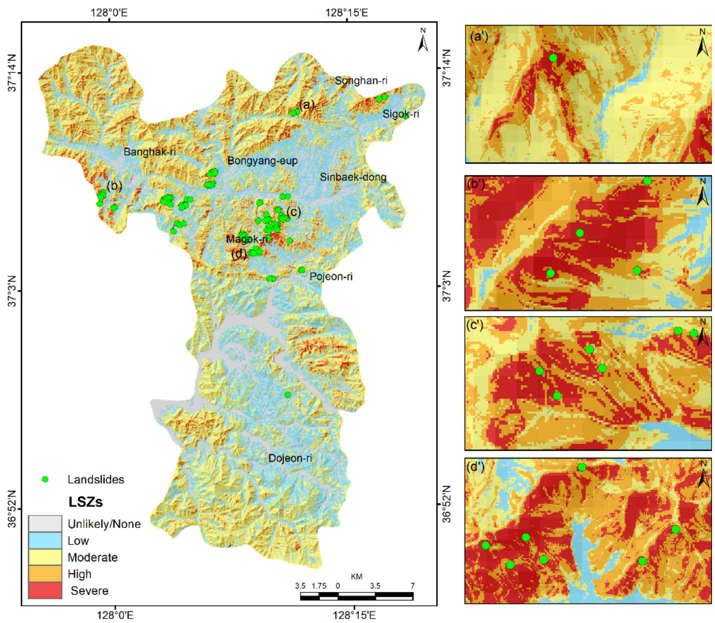

Fig. 14 a Landslide hazard microzonation map of the Jecheon-si region using a hybrid Integrated approach, while subplots **a'-d'** represent the region's detailed LSI and associated landslide inventory.

4.5 Validation of landslide hazard microzonation map based on landslide inventory and in-situ observations

Evaluating the accuracy assessment between susceptibility classes and actual landslide observations is essential, as past instability evidence often serves as the best guide for predicting future behavior in the locality. Thus, the integrated landslide hazard microzonation map was verified based on the reported and in-situ observations. We used the landslide inventory database to calculate the effectiveness of the integrated LSI method and determine the precision of the susceptibility index. Subsequently, the landslide density (Li), precision (P), MAE, MSE, RMSE, R-index, and AUC have been calculated to validate the outcome. Table 5 illustrates detailed landslide frequencies for each susceptibility zone. It was observed that the L_i values increased gradually from the unlikely to the severe susceptible classes. Additionally, L_i values vary considerably between classes. Therefore, it can be said that the developed hazard microzonation map indicates reasonable hazard classes. We also assessed the validity of the calculated LSI based on the P-value, which is the difference between the slide area in the upper low (severe to high) and the total area of the slide. The precision of our proposed methods was

https://doi.org/10.5194/egusphere-2025-1169
Preprint. Discussion started: 13 June 2025

determined to be 88.3%, which is deemed acceptable for identifying the likelihood of landslide-prone regions in this area. In addition, the R-index results indicate that the LSM has a very high prediction accuracy.

The hybrid integrated LSI model was further examined using MSE, MAE, and RMSE with the landslide inventory data. The MSE, MAE, and RMSE values for the integrated models are 0.25, 0.08, & 0.28, respectively, exhibiting good consistency with the in-situ observations. On the other hand, correct classification percentages (for 0.5 cut-off value) are also calculated to assess the LSI's sensitivity (Gorum et al., 2008). It is exhibited that the integrated models have a prediction capacity of 94.6% (Fig. 15a).

Table 5 Accuracy statistics of the landslide hazard zonation map.

<table>
<tr><th>LSZM</th><th>P_i</th><th>% P_i</th><th>L_i</th><th>% L_i</th><th>Landslide Density</th><th>R-Index</th><th>P</th><th>MAE</th><th>MSE</th><th>RMSE</th></tr>
<tr><td>Unlikely</td><td>4174356</td><td>11.82</td><td>0</td><td>0.00</td><td>0.00</td><td>0.00</td><td rowspan="5">88.3</td><td rowspan="5">0.25</td><td rowspan="5">0.08</td><td rowspan="5">0.28</td></tr>
<tr><td>Low</td><td>10661338</td><td>30.20</td><td>2</td><td>1.79</td><td>0.06</td><td>0.31</td></tr>
<tr><td>Moderate</td><td>14230579</td><td>40.31</td><td>11</td><td>9.82</td><td>0.24</td><td>1.30</td></tr>
<tr><td>High</td><td>5272713</td><td>14.94</td><td>52</td><td>46.43</td><td>3.11</td><td>16.53</td></tr>
<tr><td>Severe</td><td>962462</td><td>2.73</td><td>47</td><td>41.96</td><td>15.39</td><td>81.86</td></tr>
</table>

*LSZM-landslide susceptibility zonation map

The LSI models were also evaluated through the ROC curve analysis. The result of the ROC curve test is shown in Fig. 15b. An AUC value of 0.7 or more indicates good predictive performance (Mandal et al., 2021). The AUC values obtained from the FR, IV, CF, LR and integrated model are 0.889, 0.872, 0.877, 0.912, and 0.909, respectively, which suggests a high landslide prediction rate. Therefore, the zones of high and severe landslide susceptibility identified by all the models indicate the degree of field instability. However, the LSI predicted based on the integrated method was consistent with the topographic and landslide characteristics, suggesting more reliable and appropriate outcomes than other models.

https://doi.org/10.5194/egusphere-2025-1169
Preprint. Discussion started: 13 June 2025

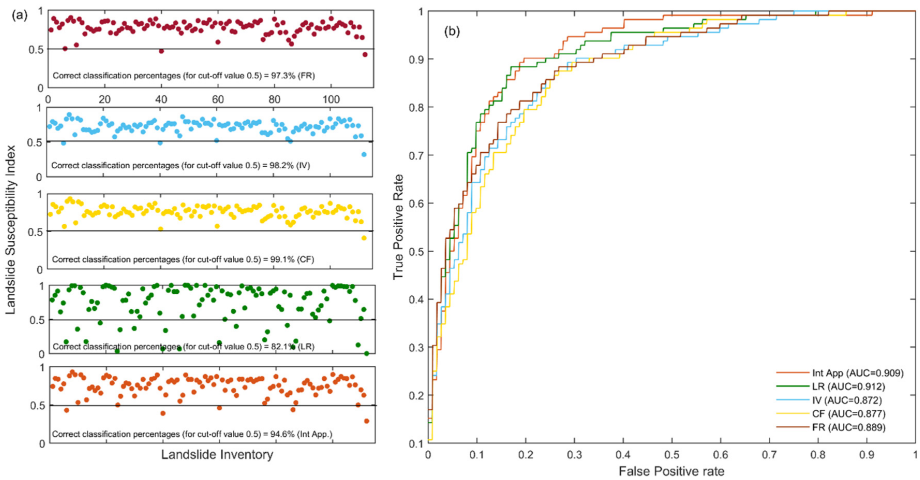

Fig. 15 a The estimated LSI of the landslide inventory datasets with correct classification percentages, and **b** Model performance based on the AUC.

5. Conclusion

Landslide susceptibility analysis requires a detailed database of landslide inventory and influencing factors. The high-resolution spatial database, comprising 18 predisposing factors, including topography, hydrology, lithology, soil, and forest aspects, was utilized to predict LSI for the Jecheon-si region of South Korea. It was observed that the IV, CF and FR models predicted higher LSI values in both the landslide source area and the landslide deposit zone. In contrast, the LR model predicted moderate LSI values in the landslide source area and lower LSI values in the landslide deposit zone. So, the four applied models can successfully and reliably predict the susceptible zones; however, the predicted LSI distributions were not always consistent with topographic and landslide characteristics. To overcome this issue, we proposed a hybrid integrated approach for better performance. It was observed that the LSI predicted through a hybrid integrated approach was consistent with the topographic and landslide characteristics, which were not present in the earlier models. After that, the LSI calculated through the hybrid integrated approach was classified into five landslide susceptibility microzones: unlikely, low, medium, high, and severe. It was observed that most landslides occurred in the very high to severe susceptible zones, with a gradual decrease toward lower susceptibility zones, which indicates the LSZ agreed with field instability. The precision results (i.e., AUC=0.906, MSE=0.0.25, MSE=0.08, RMSE=0.28, P=88.3%) suggest that the hybrid integrated approach would be useful for landcover planning and landslide induces disaster mitigation purposes. In addition, this research methodology will be helpful for the local government's disaster preventative measures and be a useful, practical reference for predicting the risk of landslides on the Korean Peninsula.

Acknowledgment

This research work was funded by the National Research Foundation, Korea (NRF) under Grant [2021R1C1C2010999]. This research work was also funded by the National Research Foundation of Korea (NRF) grant funded by the Korea government (MSIT) (NRF-2021R1C1C2003316).

References

Abd El-Raouf, A., Iqbal, I., Meister, J., Abdelrahman, K., Alzahrani, H., and Badran, O. M.: Earthflow reactivation assessment by multichannel analysis of surface waves and electrical resistivity tomography: A case study, Open Geosci., 13(1), 1328-1344, https://doi.org/10.1515/geo-2020-0310, 2021.

Achu, A. L., Aju, C. D., Pham, Q. B., Reghunath, R., and Anh, D. T.: Landslide susceptibility modelling using hybrid bivariate statistical-based machine-learning method in a highland segment of Southern Western Ghats, India, Environ. Earth Sci., 81(13), 1-18, https://doi.org/10.1007/s12665-022-10464-z, 2022.

Aditian, A., Kubota, T., and Shinohara, Y.: Comparison of GIS-based landslide susceptibility models using frequency ratio, logistic regression, and artificial neural network in a tertiary region of Ambon, Indonesia, Geomorphology, 318, 101-111, https://doi.org/10.1016/j.geomorph.2018.06.006, 2018.

Agrawal, N., and Dixit, J.: Assessment of landslide susceptibility for Meghalaya (India) using bivariate (frequency ratio and Shannon entropy) and multi-criteria decision analysis (AHP and fuzzy-AHP) models, All Earth, 34(1), 179-201, https://doi.org/10.1080/27669645.2022.2101256, 2022.

Ayalew, L., Yamagishi, H., Marui, H., and Kanno, T.: Landslides in Sado Island of Japan: Part II. GIS-based susceptibility mapping with comparisons of results from two methods and verifications, Eng. Geol., 81(4), 432-445, https://doi.org/ 10.1016/j.enggeo.2005.08.004, 2005.

Chen, W., Li, W., Hou, E., Zhao, Z., Deng, N., Bai, H., and Wang, D.: Landslide susceptibility mapping based on GIS and information value model for the Chencang District of Baoji, China, Arab. J. Geosci., 7(11), 4499-4511, https://doi.org/10.1007/ s12517-014-1369-z, 2014.

Chen, W., Panahi, M., Tsangaratos, P., Shahabi, H., Ilia, I., Panahi, S., Li, S., Jaafari, A., and Ahmad, B. B.: Applying population-based evolutionary algorithms and a neuro-fuzzy system for modeling landslide susceptibility, Catena, 172, 212-231, https://doi.org/10.1016/ j.catena.2018.08.025, 2019.

Chen, X., and Chen, W.: GIS-based landslide susceptibility assessment using optimized hybrid machine learning methods, Catena, 196, 104833, https://doi.org/

10.1016/j.catena.2020.104833, 2021.
Choi, J., Oh, H. J., Lee, H. J., Lee, C., and Lee, S.: Combining landslide susceptibility maps obtained from frequency ratio, logistic regression, and artificial neural network models using ASTER images and GIS, Eng. Geol., 124, 12-23, https://doi.org/10.1016/j.enggeo.2011.09.011, 2012.
Dash, R. K., Falae, P. O., and Kanungo, D. P.: Debris flow susceptibility zonation using statistical models in parts of Northwest Indian Himalayas-implementation, validation, and comparative evaluation, Nat. Hazards, 111(2), 2011-2058, https://doi.org/10.1007/s11069-021-05128-3, 2022.
Devkota, K. C., Regmi, A. D., Pourghasemi, H. R., Yoshida, K., Pradhan, B., Ryu, I. C., Dhital, M. R., and Althuwaynee, O. F.: Landslide susceptibility mapping using certainty factor, index of entropy and logistic regression models in GIS and their comparison at Mugling–Narayanghat road section in Nepal Himalaya, Nat. Hazards, 65(1), 135-165, https://doi.org/10.1007/s11069-012-0347-6, 2013.
Fadhillah, M. F., Hakim, W. L., Panahi, M., Rezaie, F., Lee, C. W., and Lee, S.: Mapping of landslide potential in Pyeongchang-gun, South Korea, using machine learning meta-based optimization algorithms, Egypt. J. Remote Sens. Space Sci., 25(2), 463-472, https://doi.org/10.1016/j.ejrs.2022.03.008, 2022.
Fonseca, L. D. A. M., Lani, J. L., Santos, G. R. D., Ferreira, W. P. M., and Santos, A. M. R. T.: Variability in soil physical properties in landslide-prone areas, Acta Sci-Agron., 39, 109-118, https://doi.org/10.4025/actasciagron.v39i1.30561, 2017.
Ghosh, J. K., and Bhattacharya, D.: Knowledge-based landslide susceptibility zonation system, J. Comput. Civil Eng., 24(4), 325-334, https://doi.org/ 10.1061/(ASCE)CP.1943-5487.000003, 2010.
Giarola, A., Meisina, C., Tarolli, P., Zucca, F., Galve, J. P., and Bordoni, M.: A data-driven method for the estimation of shallow landslide runout, Catena, 234,107573, https://doi.org/10.1016/j.catena.2023.107573, 2024.
Gorum, T., Gonencgil, B., Gokceoglu, C., Nefeslioglu, H. A.: Implementation of reconstructed geomorphologic units in landslide susceptibility mapping: the Melen Gorge (NW Turkey), Nat. Hazards, 46(3), 323-351, https://doi.org/10.1007/s11069-007-9190-6, 2008.
Guzzetti, F., Carrara, A., Cardinali, M., and Reichenbach, P.: Landslide hazard evaluation: a review of current techniques and their application in a multi-scale study, Central Italy, Geomorphology, 31(1-4), 181-216, https://doi.org/10.1016/S0169-555X(99)00078-1, 1999.
He, Y., Zhao, Z. A., Yang, W., Yan, H., Wang, W., Yao, S., Zhang, L., and Liu, T.: A unified network of information considering superimposed landslide factors sequence and pixel spatial neighbourhood for landslide susceptibility mapping, Int. J. Appl. Earth Obs. Geoinf., 104, 102508, https://doi.org/10.1016/ j.jag. 2021.102508, 2021.
Hong, H., Liu, J., and Zhu, A. X.: Modeling landslide susceptibility using LogitBoost alternating decision trees and forest by penalizing attributes with the bagging ensemble, Sci. Total Environ., 718, 137231, https://doi.org/10.1016/j.scitotenv. 2020.137231, 2020.
Huang, F., Cao, Z., Guo, J., Jiang, S. H., Li, S., and Guo, Z.: Comparisons of heuristic, general statistical and machine learning models for landslide susceptibility prediction and

https://doi.org/10.5194/egusphere-2025-1169
Preprint. Discussion started: 13 June 2025

mapping, Catena, 191, 104580, https://doi.org/10.1016/j.catena.2020.104580, 2020.

Huang, Y., and Zhao, L.: Review on landslide susceptibility mapping using support vector machines, Catena, 165, 520-529, https://doi.org/10.1016/j.catena.2018.03.003, 2018.

Jung, J-W., and Kang, J. H.: Geological structures in the Bonghwajae area Jecheon-si, Chungcheongbuk-do, Korea, J. Petrological Soc. Korea, 23(2), 105-117, https://doi.org/10.7854/JPSK.2014.23.2.105, 2014.

Kadavi, P. R., Lee, C. W., and Lee, S.: Application of ensemble-based machine learning models to landslide susceptibility mapping, Remote Sens., 10(8), 1252, https://doi.org/10.3390/rs10081252, 2018.

Kadavi, P. R., Lee, C. W., and Lee, S.: Landslide-susceptibility mapping in Gangwon-do, South Korea, using logistic regression and decision tree models, Environ. Earth Sci., 78(4), 1-17, https://doi.org/10.1007/s12665-019-8119-1, 2019.

Kihm, Y. H., Kim, J. H., and Cheong, S. W.: Geological structures of the Southern Jecheon, Korea: Uplift process of Dangdusan metamorphic complex and its implication, J. Korean Earth Sci. Soc., 21(3), 302-314, 2000.

Kim, S. W., Chun, K. W., Kim, M., Catani, F., Choi, B., and Seo, J. I.: Effect of antecedent rainfall conditions and their variations on shallow landslide-triggering rainfall thresholds in South Korea, Landslides, 18(2), 569-582, https://doi.org/10.1007/s10346-020-01505-4, 2021.

Lee, J. H., Sameen, M. I., Pradhan, B., and Park, H. J.: Modeling landslide susceptibility in data-scarce environments using optimized data mining and statistical methods, Geomorphology, 303, 284-298, https://doi.org/10.1016/j.geomorph.2017.12.007, 2018.

Lee, J. U., Cho, Y. C., Kim, M., Jang, S. J., Lee, J., and Kim, S.: The Effects of Different Geological Conditions on Landslide-Triggering Rainfall Conditions in South Korea, Water, 14(13), 2051, https://doi.org/10.3390/w14132051, 2022a.

Lee, J. J., Song, M. S., Yun, H. S., and Yum, S. G.: Dynamic landslide susceptibility analysis that combines rainfall period, accumulated rainfall, and geospatial information, Sci. Rep., 12(1), 1-20, https://doi.org/10.1038/s41598-022-21795-z, 2022b.

Lee, M. J., Park, I., and Lee, S.: Forecasting and validation of landslide susceptibility using an integration of frequency ratio and neuro-fuzzy models: a case study of Seorak mountain area in Korea, Environ. Earth Sci., 74(1), 413-429, https://doi.org/10.1007/s12665-015-4048-9, 2015.

Lee, S. G., and Winter, M. G. The effects of debris flow in the Republic of Korea and some issues for successful risk reduction, Eng. Geology, 251,172-189, https://doi.org/10.1016/j.enggeo.2019.01.003, 2019.

Lee, S., and Min, K.: Statistical analysis of landslide susceptibility at Yongin, Korea, Environ. Geol., 40(9), 1095-1113, https://doi.org/10.1007/s002540100310, 2001.

Lee, S., and Pradhan, B.: Landslide hazard mapping at Selangor, Malaysia using frequency ratio and logistic regression models, Landslides, 4, 33–41, https://doi.org/10.1007/s10346-006-0047-y , 2007.

Lee, S., and Talib, J. A.: Probabilistic landslide susceptibility and factor effect analysis, Environ. Geol., 47(7), 982-990, https://doi.org/10.1007/s00254-005-1228-z, 2005.

Lee, S., Choi, J., and Min, K.: Probabilistic landslide hazard mapping using GIS and remote

https://doi.org/10.5194/egusphere-2025-1169
Preprint. Discussion started: 13 June 2025

sensing data at Boun, Korea, Int. J. Remote Sens., 25(11), 2037-2052, https://doi.org/10.1080/01431160310001618734, 2004.

Lee, S., Chwae, U., and Min, K.: Landslide susceptibility mapping by correlation between topography and geological structure: the Janghung area, Korea, Geomorphology, 46(3-4), 149-162, https://doi.org/10.1016/S0169-555X(02)00057-0, 2002.

Lee, S., Hong, S. M., and Jung, H. S.: A support vector machine for landslide susceptibility mapping in Gangwon Province, Korea, Sustainability, 9(1), 48, https://doi.org/10.3390/su9010048, 2017.

Lee, S.: Application of logistic regression model and its validation for landslide susceptibility mapping using GIS and remote sensing data, Int. J. Remote Sens., 26, 1477–1491, https://doi.org/10.1080/01431160412331331012, 2005.

Mandal, K., Saha, S., and Mandal, S.: Applying deep learning and benchmark machine learning algorithms for landslide susceptibility modelling in Rorachu river basin of Sikkim Himalaya, India, Geosci. Front., 12(5), 10120, https://doi.org/ 10.1016/j.gsf.2021.101203, 2021.

Martinello, C., Cappadonia, C., Conoscenti, C., and Rotigliano, E.: Landform classification: a high-performing mapping unit partitioning tool for landslide susceptibility assessment—a test in the Imera River basin (northern Sicily, Italy), Landslides, 19(3), 539-553, https://doi.org/10.1007/s10346-021-01781-8, 2022.

Merghadi, A., Yunus, A. P., Dou, J., Whiteley, J., ThaiPham, B., Bui, D. T., Avtar, R., and Abderrahmane, B.: Machine learning methods for landslide susceptibility studies: A comparative overview of algorithm performance, Earth Sci. Rev., 207, 103225, https://doi.org/10.1016/j.earscirev.2020.103225, 2020.

Oh, H. J., Kadavi, P. R., Lee, C. W., and Lee, S.: Evaluation of landslide susceptibility mapping by evidential belief function, logistic regression and support vector machine models, Geomat. Nat. Hazards Risk., 9(1), 1053-1070, https://doi.org/10.1080/19475705.2018.1481147, 2018.

Oh, H. J., and Lee, S.: Shallow landslide susceptibility modeling using the data mining models artificial neural network and boosted tree, Appl. Sci., 7(10), 1000, https://doi.org/10.3390/app7101000, 2017.

Panahi, M., Gayen, A., Pourghasemi, HR., Rezaie, F., and Lee, S.: Spatial prediction of landslide susceptibility using hybrid support vector regression (SVR) and the adaptive neuro-fuzzy inference system (ANFIS) with various metaheuristic algorithms. Sci. Total Environ., 741, 139937, https://doi.org/10.1016/j.scitotenv.2020.139937, 2020.

Park, S., Choi, C., Kim, B., and Kim, J.: Landslide susceptibility mapping using frequency ratio, analytic hierarchy process, logistic regression, and artificial neural network methods at the Inje area, Korea. Environ. Earth Sci. 68(5), 1443-1464, https://doi.org/10.1007/s12665-012-1842-5, 2013.

Park, S., Hamm, S. Y., and Kim, J.: Performance evaluation of the GIS-based data-mining techniques decision tree, random forest, and rotation forest for landslide susceptibility modeling, Sustainability 11(20), 5659, https://doi.org/10.3390/su11205659, 2019.

Peethambaran, B., and Leshchinsky, B.: Application of landslide susceptibility towards urbanization suitability zonation in mountainous settings, Int. J. Disaster Risk Reduct., 97, 104061, https://doi.org/10.1016/j.ijdrr.2023.104061, 2023.

Petschko, H., Brenning, A., Bell, R., Goetz, J., and Glade, T.: Assessing the quality of landslide susceptibility maps–case study Lower Austria, Nat. Hazards Earth Syst. Sci., 14(1), 95-118, https://doi.org/10.5194/nhess-14-95-2014, 2014.

Pham, B. T., Prakash, I., Dou, J., Singh, S. K., Trinh, P. T., Tran, H. T., Le, T. M., Phong, T. V., Khoi, D. K., Shirzadi, A., and Bui, D. T.: A novel hybrid approach of landslide susceptibility modelling using rotation forest ensemble and different base classifiers, Geocarto Int., 35(12), 1267-1292, https://doi.org/10.1080/10106049.2018.1559885, 2020.

Pradhan, A. M. S., and Kim, Y. T.: Evaluation of a combined spatial multi-criteria evaluation model and deterministic model for landslide susceptibility mapping, Catena, 140, 125-139, https://doi.org/10.1016/j.catena.2016.01.022, 2016.

Pradhan, A. M. S., and Kim, Y. T.: Relative effect method of landslide susceptibility zonation in weathered granite soil: a case study in Deokjeok-ri Creek, South Korea, Nat. Hazards, 72(2), 1189-1217, https://doi.org/10.1007/s11069-014-1065-z, 2014.

Qiu, H., Cui, P., Regmi, A. D., Hu, S., Wang, X., and Zhang, Y.: The effects of slope length and slope gradient on the size distributions of loess slides: Field observations and simulations, Geomorphology, 300, 69-76, https://doi.org/10.1016/j.geomorph.2017.10.020, 2018.

Reichenbach, P., Rossi, M., Malamud, B. D., Mihir, M., and Guzzetti, F.: A review of statistically-based landslide susceptibility models, Earth Sci. Rev., 180, 60-91, https://doi.org/10.1016/j.earscirev.2018.03.001, 2018.

Riaz, M. T., Basharat, M., Hameed, N., Shafique, M., and Luo, J.: A data-driven approach to landslide-susceptibility mapping in mountainous terrain: case study from the Northwest Himalayas, Pakistan, Nat. Hazards Rev., 19(4), 05018007, https://doi.org/10.1061/(ASCE)NH.1527-6996.0000302, 2018.

Saha, S., Sarkar, R., Roy, J., Hembram, T. K., Acharya, S., Thapa, G., and Drukpa, D.: Measuring landslide vulnerability status of Chukha, Bhutan using deep learning algorithms, Sci. Rep., 11(1), 1-23, https://doi.org/10.1038/s41598-021-95978-5, 2021.

Sameen, M. I., Pradhan, B., and Lee, S.: Application of convolutional neural networks featuring Bayesian optimization for landslide susceptibility assessment, Catena, 186, 104249, https://doi.org/10.1016/j.catena.2019.104249, 2020.

Sarkar, S., Roy, A. K., and Martha, T. R.: Landslide susceptibility assessment using information value method in parts of the Darjeeling Himalayas, J. Geol. Soc. India, 82(4), 351-362, https://doi.org/10.1007/s12594-013-0162-z, 2013.

Seo, J. A., Kim, Y. C., Kim, J. S., and Kim, Y. J.: Site prioritization for artificial recharge in Korea using GIS mapping, J. Soil Groundwater Environ., 16(6), 66-78, https://doi.org/10.7857/JSGE.2011.16.6.066, 2011.

Shahabi, H., and Hashim, M.: Landslide susceptibility mapping using GIS-based statistical models and Remote sensing data in tropical environment, Sci. Rep., 5(1), 1-15, https://doi.org/10.1038/srep09899 , 2015.

Shano, L., Raghuvanshi, T. K., and Meten, M.: Landslide susceptibility evaluation and hazard zonation techniques–a review, Geoenviron. Disasters, 7(1), 1-19, https://doi.org/10.1186/s40677-020-00152-0, 2020.

https://doi.org/10.5194/egusphere-2025-1169
Preprint. Discussion started: 13 June 2025

Shirzadi, A., Bui, D. T., Pham, B. T., Solaimani, K., Chapi, K., Kavian, A., Shahabi, H., Revhaug, I.: Shallow landslide susceptibility assessment using a novel hybrid intelligence approach, Environ. Earth Sci., 76(2), 1-18, https://doi.org/10.1007/s12665-016-6374-y, 2017.

Sonker, I., Tripathi, J. N., and Swarnim: Remote sensing and GIS-based landslide susceptibility mapping using frequency ratio method in Sikkim Himalaya, Quat. Sci. Adv., 8, 100067, https://doi.org/10.1016/j.qsa.2022.100067, 2022.

Trinh, T., Luu, B. T., Le, T. H. T., Nguyen, D. H., Van Tran, T., Van Nguyen, T. H., Nguyen, K. Q., and Nguyen, L. T.: A comparative analysis of weight-based machine learning methods for landslide susceptibility mapping in Ha Giang area, Big Earth Data, 1-30, https://doi.org/10.1080/20964471.2022.2043520, 2022.

Van Den Eeckhaut, M., Hervás. J., Jaedicke, C., Malet, J. P., Montanarella, L., and Nadim, F.: Statistical modelling of Europe-wide landslide susceptibility using limited landslide inventory data, Landslides, 9(3), 357-369, https://doi.org/10.1007/s10346-011-0299-z, 2012.

Wald, D. J., and Allen, T. I.: Topographic slope as a proxy for seismic site conditions and amplification, Bull. Seismol. Soc. Am. 97(5), 1379-1395, https://doi.org/10.1785/0120060267, 2007.

Wang, L. J., Guo, M., Sawada, K., Lin, J., and Zhang, J.: Landslide susceptibility mapping in Mizunami City, Japan: A comparison between logistic regression, bivariate statistical analysis and multivariate adaptive regression spline models, Catena, 135, 271-282, https://doi.org/10.1016/j.catena.2015.08.007, 2015.

Wang, Q., Guo, Y., Li, W., He, J., and Wu, Z.: Predictive modeling of landslide hazards in Wen County, northwestern China based on information value, weights-of-evidence, and certainty factor, Geomat. Nat. Hazards Risk, 10(1), 820-835, https://doi.org/10.1080/19475705.2018.1549111, 2019.

Wei, X., Zhang, L., Gardoni, P., Chen, Y., Tan, L., Liu, D., Du, C., and Li, H.: Comparison of hybrid data-driven and physical models for landslide susceptibility mapping at regional scales, Acta Geotech., 18, 4453-4476, https://doi.org/10.1007/s11440-023-01841-4, 2023.

Yilmaz, I.: Landslide susceptibility mapping using frequency ratio, logistic regression, artificial neural networks and their comparison: a case study from Kat landslides (Tokat-Turkey), Comput. Geosci., 35(6), 1125-1138, https://doi.org/10.1016/j.cageo.2008.08.007, 2009.

Yin, K. L., and Yan, T. Z.: Statistical prediction model for slope instability of metamorphosed rocks. *In: Proceedings of the 5th international symposium on landslides*, Lausanne, Switzerland, 2, 1269–1272, 1988.

Zêzere, J. L., Pereira, S., Melo, R., Oliveira, S. C., and Garcia, R. A.: Mapping landslide susceptibility using data-driven methods, Sci. Total Environ., 589, 250-267, https://doi.org/10.1016/j.scitotenv.2017.02.188, 2017.

Zhang, Y., Wu, W., Qin, Y., Lin, Z., Zhang, G., Chen, R., et al.: Mapping landslide hazard risk using random forest algorithm in Guixi, Jiangxi, China, ISPRS Int. J. Geo-Inf., 9(11), 695, https://doi.org/10.3390/ijgi9110695, 2020.

Zhou, C., Yin, K., Cao, Y., Ahmed, B., Li, Y., Catani, F., and Pourghasemi, H. R.: Landslide

https://doi.org/10.5194/egusphere-2025-1169
Preprint. Discussion started: 13 June 2025

susceptibility modeling applying machine learning methods: A case study from Longju in the Three Gorges Reservoir area, China, Comput. Geosci. 112, 23-37, https://doi.org/10.1016/j.cageo.2017.11.019, 2018.

Zhou, X., Wu, W., Qin, Y., and Fu, X.: Geoinformation-based landslide susceptibility mapping in subtropical area, Sci. Rep., 11(1), 1-16, https://doi.org/10.1038/ s41598-021-03743-5, 2021.

Zhu, A. X., Miao, Y., Wang, R., Zhu, T., Deng, Y., Liu, J., Yang, L., Qin, C. Z., and Hong, H.: A comparative study of an expert knowledge-based model and two data-driven models for landslide susceptibility mapping, Catena, 166, 317-327, https://doi.org/10.1016/j.catena.2018.04.003, 2018.